6-1-2012

Polarization-analyzed small-angle neutron scattering. II. Mathematical angular analysis

Kathryn L. Krycka

Julie A. Borchers

Yumi Ijiri
Oberlin College, Yumi.Ijiri@oberlin.edu

R. A. Booth

S. A. Majetich

Repository Citation

Polarization-analyzed small-angle neutron scattering. II. Mathematical angular analysis

Kathryn Krycka, Julie Borchers, Yumi Ijiri, Ryan Booth and Sara Majetich
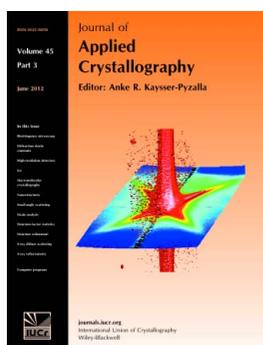
Journal of Applied Crystallography covers a wide range of crystallographic topics from the viewpoints of both techniques and theory. The journal presents papers on the application of crystallographic techniques and on the related apparatus and computer software. For many years, the *Journal of Applied Crystallography* has been the main vehicle for the publication of small-angle scattering papers and powder diffraction techniques. The journal is the primary place where crystallographic computer program information is published.

Crystallography Journals Online is available from journals.iucr.org

Polarization-analyzed small-angle neutron scattering. II. Mathematical angular analysis

Kathryn Krycka,[a]* Julie Borchers,[a] Yumi Ijiri,[b] Ryan Booth[c] and Sara Majetich[c]

[a]NIST Center for Neutron Research, National Institute of Standards and Technology, Gaithersburg, MD, USA, [b]Department of Physics and Astronomy, Oberlin College, Oberlin, OH, USA, and [c]Department of Physics, Carnegie Mellon University, Pittsburgh, PA, USA. Correspondence e-mail: kathryn.krycka@nist.gov

Polarization-analyzed small-angle neutron scattering (SANS) is a powerful tool for the study of magnetic morphology with directional sensitivity. Building upon polarized scattering theory, this article presents simplified procedures for the reduction of longitudinally polarized SANS into terms of the three mutually orthogonal magnetic scattering contributions plus a structural contribution. Special emphasis is given to the treatment of anisotropic systems. The meaning and significance of scattering interferences between nuclear and magnetic scattering and between the scattering from magnetic moments projected onto distinct orthogonal axes are discussed in detail. Concise tables summarize the algorithms derived for the most commonly encountered conditions. These tables are designed to be used as a reference in the challenging task of extracting the full wealth of information available from polarization-analyzed SANS.

1. Introduction

Small-angle neutron scattering (SANS) with polarization analysis is a powerful tool for studying magnetism on the nanoscale because it can be utilized to unambiguously separate the structural and magnetic scattering contributions with sensitivity to the direction of the magnetic spins. Unlike bulk probes, this technique measures magnetic structures aligned both parallel and perpendicular to an external magnetic guide field and, notably, it is sensitive to the presence of magnetic domains, even those that average to zero across the sample. Additionally, this technique is nondestructive, provides sub-nanometre resolution, and has the ability to penetrate deeply into materials to probe the ensemble-averaged properties spanning local magnetic morphology to collective magnetic responses. Moreover, recent developments in the degree of polarization within ^{3}He neutron spin filters (Petoukhov et al., 2006; Babcock et al., 2007; Keiderling et al., 2008; Chen et al., 2009), which allow the neutron spins from a divergently scattered beam to be assayed, have sparked renewed interest in polarized SANS (e.g. Cywinski et al., 1999; Wiedenmann, 2005; Michels & Weissmüller, 2008; Feygenson et al., 2010; Laver et al., 2010; Krycka et al., 2010; Chang et al., 2010; Honecker et al., 2011; Dufour et al., 2011). The theory of polarized neutron scattering was derived by Halpern & Johnson (1939), refined by Blume (1963) and Maleyev et al. (1963), and adapted for longitudinal polarization analysis (i.e. with a magnetic guide field that is used to define the direction of the neutron polarization axis, $\hat{\mathbf{p}}$) by Moon et al. (1969).[1]

Additional treatments that utilize a combination of applied field directions are provided by Schärpf & Capellmann (1993) and Schweika (2010). If the incident neutron beam is polarized, but the scattered neutron beam spin is not analyzed, it is usually referred to as half-polarization or SANSPOL (Wiedenmann, 2005). Neutron spin analysis of both the incident and the scattered longitudinally polarized neutrons has been referred to as *XYZ* polarization (Schärpf & Capellmann, 1993; Schweika, 2010) in the general case and as POLARIS (Wiedenmann, 2005; Keiderling et al., 2008) when applied to SANS, but for simplicity we shall refer to it here generically as polarization-analyzed SANS (PASANS).

Although the theory of polarized SANS is well established, the complex combination of structural and directionally sensitive magnetic scattering terms plus their interferences can be daunting to disentangle and analyze. This is especially true for the class of samples that may be structurally or magnetically anisotropic (e.g. solvated magnetic nanoparticles that form chains in response to application of a magnetic field or shearing force). Two approaches have been adopted to analyze PASANS data: (1) to reproduce the combined structural and magnetic scattering patterns from micromagnetic models (Löffler et al., 2005; Ogrin et al., 2006; Michels & Weissmüller, 2008; Saranu et al., 2008) and (2) to separate the structural from the magnetic scattering in terms of the three mutually orthogonal magnetic scattering contributions (Schärpf & Capellmann, 1993; Schweika, 2010). Both approaches have their merits and may be highly complementary. The latter, however, is quite powerful for samples with largely unknown magnetic structures as it provides a great deal of user insight into the underlying order and it facilitates the choice of the most appropriate models. Such an analysis also helps to ensure that, in situations in which the scattering contribution from moments aligned perpendicular

---

[1] Spherical neutron polarimetry (SNP), in which scattering occurs within a nearly perfect zero magnetic field environment, has been developed by Tasset (1989) and Brown (2001). Here the neutron spin is free to rotate upon scattering, whereas in longitudinal polarization the neutron spins precess about $\hat{\mathbf{p}}$ with a projection either parallel to or antiparallel to $\hat{\mathbf{p}}$ at all times. SNP shall not be considered further within this manuscript.

to the neutron polarization axis is relatively small yet important, fine magnetic details are not lost within the global modeling process.

Thus, the intent of this article is to compute, simplify and summarize the procedures required to reduce longitudinally polarization-analyzed SANS scattering contributions into terms of the three mutually orthogonal magnetic scattering contributions plus a structural contribution. We give special emphasis to the treatment of systems that may be anisotropic as a function of $\mathbf{Q}$, the scattering wavevector [$Q = |\mathbf{Q}| = (4\pi/\lambda)\sin(\theta/2)$, where θ is the scattering angle and λ is the wavelength of the incident radiation], and develop specific algorithms for the most commonly encountered conditions. We also investigate the meaning and significance of interferences both between nuclear and magnetic scattering and between the scattering from magnetic moments projected onto distinct orthogonal axes. Finally, we discuss circumstances in which the existence or lack of a relationship between terms can be used to further reduce and interpret the polarization-analyzed data. The tables derived and provided here are designed to be used as a handy reference to aid in the challenging task of extracting the full wealth of information available from polarization-analyzed SANS.

2. PASANS setup

A typical (longitudinal) PASANS setup is shown in Fig. 1, with the incident beam along the Z axis, the neutron spin polarization oriented along the X axis (as shown) or Z axis, and a position-sensitive gas detector set in the XY plane. The application of a magnetic guide field (which in practical terms may be as small as several Gauss) defines $\hat{\mathbf{p}}$ about which the neutrons precess at the Larmor frequency. For an unpolarized incident neutron beam, half of the neutron spins will have a projection parallel to $\hat{\mathbf{p}}$ ($\uparrow$) and half antiparallel to $\hat{\mathbf{p}}$ ($\downarrow$). The

neutron beam may be polarized by sending it through a supermirror cavity that preferentially reflects only one of these spin states ($\uparrow$). (The polarization of the neutron beam is defined as $(\mathbb{N}^{\uparrow} - \mathbb{N}^{\downarrow})/(\mathbb{N}^{\uparrow} + \mathbb{N}^{\downarrow})$, where $\mathbb{N}^{\uparrow}$ and $\mathbb{N}^{\downarrow}$ denote the number of neutrons found in the $\uparrow$ or $\downarrow$ state, respectively.) The neutron spins adiabatically follow the applied magnetic guide field, even as it changes direction along the neutron beam path, as long as $\hat{\mathbf{p}}$ remains continuously well defined and the precessional Larmor frequency of the neutron is significantly higher than the rate of rotation of the guide field within the neutron's reference frame. In contrast, an electromagnetic precession coil flipper is designed to flip (reverse by 180°) the neutron spins that pass though. This is performed by abrupt rotation of the polarization axis (i.e. nearly instantaneous in comparison with the Larmor frequency of the neutron) to an orthogonal direction and then back again, with the applied magnetic field, neutron speed and distance between these two polarization axis transformations precisely balanced so that the neutrons precess about this orthogonal axis by exactly π radians. Interaction with any magnetic moments present in the sample also provides an abrupt change in the magnetic environment, and this can lead to a flipping (180° reversal) of the spin direction of the scattered neutron, depending on the relative orientations of $\hat{\mathbf{p}}$, $\mathbf{Q}$ and the sample magnetic moment (discussed in detail in the next section). Coherent nuclear scattering (or structural scattering), which contains information about the spatial arrangement of the nuclei, does not cause neutron spin flipping, and this is the basis for the separation of structural and magnetic scattering. Finally, after interaction with the sample, the neutrons pass through a polarized ^{3}He filter (analyzer) (Petoukhov et al., 2006; Babcock et al., 2007; Keiderling et al., 2008; Chen et al., 2009). This filter is filled with a gas containing ^{3}He atoms, which each possess a spin that aligns with the applied magnetic guide field direction. This analyzer works by preferentially allowing neutrons with spin oriented in the same direction as the ^{3}He atoms to pass through, but is highly absorbing of those neutrons with spin antiparallel to the ^{3}He atoms (combining to form spin-neutral ^{4}He). The orientation of the polarized ^{3}He atoms may be reversed using a tuned nuclear magnetic resonance pulse (Jones et al., 2006) with negligible loss of polarization. After correcting for efficiencies of the polarizing elements (Majkrzak, 1991; Keiderling, 2002; Wildes, 2006; Krycka et al., 2012), this setup allows four scattering cross sections ($\sigma^{\uparrow\uparrow}$, $\sigma^{\downarrow\uparrow}$, $\sigma^{\downarrow\downarrow}$, $\sigma^{\uparrow\downarrow}$) to be measured experimentally, where the first arrow refers to the incident spin and the second arrow to the scattered spin.
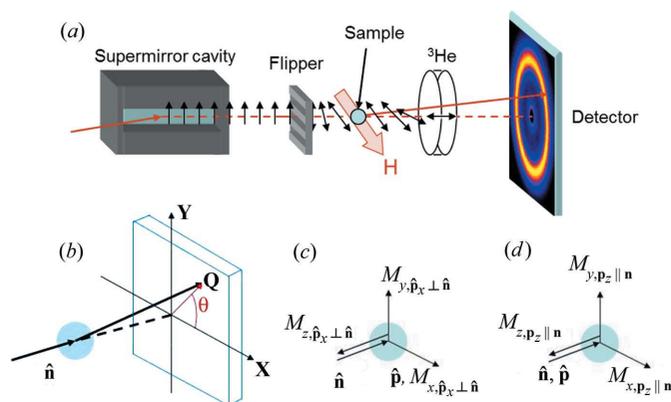
Figure 1
(a) The PASANS setup includes a polarizing supermirror, an electromagnetic precession coil flipper, a sample holder with cryostat and variable magnetic field, a ^{3}He analyzer, and a position-sensitive gas detector. Arrows indicate the neutron polarization direction, which follows the applied magnetic field, rotating from vertical to horizontal to along $\hat{\mathbf{n}}$ between the flipper, sample and ^{3}He analyzer, respectively. (b) Coordinate axes with $\hat{\mathbf{n}} \parallel \mathbf{z}$. (c), (d) Magnetic definitions for $\hat{\mathbf{p}}$ (along $\mathbf{x}$) $\perp \hat{\mathbf{n}}$ and $\hat{\mathbf{p}}$ (along $\mathbf{z}$) $\parallel \hat{\mathbf{n}}$, respectively.

3. Mathematics of PASANS

The scattering cross section, σ, is proportional to the squared absolute value of the spatial Fourier transform (i.e. the scattering amplitude; Chatterji, 2006) of the structural (i.e. nuclear) and magnetic scattering length density, $\rho_{N,M}$, defined as

$$N, M_J(\mathbf{Q}) = \sum_K \rho_{N,M_J}(K) \exp(i\mathbf{Q} \cdot \mathbf{R}_K), \qquad (1)$$

where J is any Cartesian coordinate and $\mathbf{R}_K$ is the relative position of the Kth scatterer. If a sample consists of multiple repeated structures, it is often convenient to think of the scattering amplitude as the product of the form factor (*i.e.* the Fourier transform from scattering centers within just one scattering unit) multiplied by the structure factor (*i.e.* the Fourier transform of the relative locations at which the scattering units reside).

As noted previously, scattering from magnetic moments, but not from purely structural scattering, can flip the neutron spin. In principle, ordered nuclear spins can also contribute to the scattering cross sections (Moon *et al.*, 1969). However, except in the case of extreme environmental conditions, nuclear spins are normally randomly oriented (as assumed here). The presence of random nuclear spins can readily produce incoherent scattering, as in the classic case of hydrogen scattering. Fortunately, incoherent scattering is directly measurable as a $\frac{2}{3}$ spin-flip to $\frac{1}{3}$ non-spin-flip scattering contribution, which we shall assume either is negligible or has been measured and accounted for (Gentile *et al.*, 2000; Wildes, 2006; Gaspar *et al.*, 2010).

The way in which the magnetic moments within a sample rotate (flip) the neutron spin upon scattering are governed by two general rules. First, only the component of a magnetic moment (or for our purposes the magnetic scattering amplitude, $\mathbf{M}$) that is perpendicular to $\mathbf{Q}$ may participate in neutron scattering, and this is embodied by the Halpern–Johnson vector, $\boldsymbol{\Upsilon}$ (Halpern & Johnson, 1939). The calculation consists of subtracting the projection of $\mathbf{M}$ onto the $\mathbf{Q}$ axis from $\mathbf{M}$ as

$$\boldsymbol{\Upsilon}(\hat{\mathbf{Q}}) = \mathbf{M} - (\hat{\mathbf{Q}} \cdot \mathbf{M})\,\hat{\mathbf{Q}} = |\mathbf{M}|\,[\hat{\mathbf{M}} - (\hat{\mathbf{Q}} \cdot \hat{\mathbf{M}})\,\hat{\mathbf{Q}}]. \qquad (2)$$

For many purposes, it is conceptually simpler to define $\mathbf{M}$ in terms of three orthogonal axes labeled A, B and C, where $\mathbf{A} \parallel \hat{\mathbf{p}}$ and $\mathbf{B} \times \mathbf{C} = \mathbf{A}$. This may be more succinctly written as

$$\Upsilon_{J=A,B,C}(\hat{\mathbf{Q}}) = \sum_{L=A,B,C} M_L[\cos(\omega_{L,J}) - \cos(\omega_{\mathbf{Q},J})\cos(\omega_{\mathbf{Q},L})], \qquad (3)$$

where ω denotes the angle between the subscripted variables, and can be further reduced solely into terms of θ, the angle made by $\mathbf{Q}$ and the x axis (Fig. 1).

The second rule is that, of the magnetic moment component perpendicular to $\mathbf{Q}$ (already defined by $\boldsymbol{\Upsilon}$), the portion that lies along the neutron polarization axis, $\hat{\mathbf{p}}$, contributes to non-spin-flip scattering ($\uparrow$ to $\uparrow$, or $\downarrow$ to $\downarrow$), while the remaining portion ($\perp \hat{\mathbf{p}}$) produces spin-flip scattering ($\uparrow$ to $\downarrow$, or $\downarrow$ to $\uparrow$). Taking into account handedness, mathematically this becomes (Moon *et al.*, 1969)

$$\sigma^{\downarrow\downarrow}_{\uparrow\uparrow}(\mathbf{Q}) = \tfrac{1}{2}\big|N \pm \Upsilon_A\big|^2,$$
$$\sigma^{\uparrow\downarrow}_{\downarrow\uparrow}(\mathbf{Q}) = \tfrac{1}{2}|(-\Upsilon_B \mp i\Upsilon_C)|^2. \qquad (4)$$

In the expression for $\sigma^{\uparrow\downarrow}_{\downarrow\uparrow}$, the imaginary Υ_C term indicates that Υ_C is shifted in phase by 90° from Υ_B, and the two components add in quadrature.

4. Two polarization geometries: $\hat{\mathbf{p}} \perp \hat{\mathbf{n}}$ and $\hat{\mathbf{p}} \parallel \hat{\mathbf{n}}$

We shall focus on two standard geometries: $\hat{\mathbf{p}} \perp \hat{\mathbf{n}}$ (Fig. 1c) and $\hat{\mathbf{p}} \parallel \hat{\mathbf{n}}$ (Fig. 1d). We assume that $\hat{\mathbf{n}} \parallel \hat{\mathbf{z}}$ and define $\hat{\mathbf{x}}$ to coincide with $\hat{\mathbf{p}}$ whenever $\hat{\mathbf{p}} \perp \hat{\mathbf{n}}$. Thus, θ is the angle $\mathbf{Q}$ makes with both $\hat{\mathbf{x}}$ and $\hat{\mathbf{p}}$.

For the $\hat{\mathbf{p}} \perp \hat{\mathbf{n}}$ geometry (where $Q_z = 0$), equation (3) becomes

$$\Upsilon_A(\mathbf{Q}) = M_A \sin^2(\theta) - M_B \sin(\theta)\cos(\theta),$$
$$\Upsilon_B(\mathbf{Q}) = M_B \cos^2(\theta) - M_A \sin(\theta)\cos(\theta), \qquad (5)$$
$$\Upsilon_C(\mathbf{Q}) = M_C.$$

For clarity, redefining M_A, M_B and M_C as $M_{x,\hat{\mathbf{p}}_x\perp\hat{\mathbf{n}}}$, $M_{y,\hat{\mathbf{p}}_x\perp\hat{\mathbf{n}}}$ and $M_{z,\hat{\mathbf{p}}_x\perp\hat{\mathbf{n}}}$, respectively, in combination with equations (4) and (5) produces

$$\begin{aligned}
\sigma^{\downarrow\downarrow}_{\uparrow\uparrow,\hat{\mathbf{p}}_x\perp\hat{\mathbf{n}}}(\mathbf{Q}) &= N(\mathbf{Q})N^*(\mathbf{Q}) + M_{x,\hat{\mathbf{p}}_x\perp\hat{\mathbf{n}}}(\mathbf{Q})M^*_{x,\hat{\mathbf{p}}_x\perp\hat{\mathbf{n}}}(\mathbf{Q})\sin^4(\theta) \\
&\quad + M_{y,\hat{\mathbf{p}}_x\perp\hat{\mathbf{n}}}(\mathbf{Q})M^*_{y,\hat{\mathbf{p}}_x\perp\hat{\mathbf{n}}}(\mathbf{Q})\cos^2(\theta)\sin^2(\theta) \\
&\quad - [M_{x,\hat{\mathbf{p}}_x\perp\hat{\mathbf{n}}}(\mathbf{Q})M^*_{y,\hat{\mathbf{p}}_x\perp\hat{\mathbf{n}}}(\mathbf{Q}) \\
&\quad + M^*_{x,\hat{\mathbf{p}}_x\perp\hat{\mathbf{n}}}(\mathbf{Q})M_{y,\hat{\mathbf{p}}_x\perp\hat{\mathbf{n}}}(\mathbf{Q})]\sin^3(\theta)\cos(\theta) \\
&\quad \pm [N(\mathbf{Q})M^*_{x,\hat{\mathbf{p}}_x\perp\hat{\mathbf{n}}}(\mathbf{Q}) + N^*(\mathbf{Q})M_{x,\hat{\mathbf{p}}_x\perp\hat{\mathbf{n}}}(\mathbf{Q})]\sin^2(\theta) \\
&\quad \mp [N(\mathbf{Q})M^*_{y,\hat{\mathbf{p}}_x\perp\hat{\mathbf{n}}}(\mathbf{Q}) + N^*(\mathbf{Q})M_{y,\hat{\mathbf{p}}_x\perp\hat{\mathbf{n}}}(\mathbf{Q})]\sin(\theta)\cos(\theta),
\end{aligned}$$

$$\begin{aligned}
\sigma^{\uparrow\downarrow}_{\downarrow\uparrow,\hat{\mathbf{p}}_x\perp\hat{\mathbf{n}}}(\mathbf{Q}) &= M_{z,\hat{\mathbf{p}}_x\perp\hat{\mathbf{n}}}(\mathbf{Q})M^*_{z,\hat{\mathbf{p}}_x\perp\hat{\mathbf{n}}}(\mathbf{Q}) \\
&\quad + M_{y,\hat{\mathbf{p}}_x\perp\hat{\mathbf{n}}}(\mathbf{Q})M^*_{y,\hat{\mathbf{p}}_x\perp\hat{\mathbf{n}}}(\mathbf{Q})\cos^4(\theta) \\
&\quad + M_{x,\hat{\mathbf{p}}_x\perp\hat{\mathbf{n}}}(\mathbf{Q})M^*_{x,\hat{\mathbf{p}}_x\perp\hat{\mathbf{n}}}(\mathbf{Q})\sin^2(\theta)\cos^2(\theta) \\
&\quad - [M_{x,\hat{\mathbf{p}}_x\perp\hat{\mathbf{n}}}(\mathbf{Q})M^*_{y,\hat{\mathbf{p}}_x\perp\hat{\mathbf{n}}}(\mathbf{Q}) \\
&\quad + M^*_{x,\hat{\mathbf{p}}_x\perp\hat{\mathbf{n}}}(\mathbf{Q})M_{y,\hat{\mathbf{p}}_x\perp\hat{\mathbf{n}}}(\mathbf{Q})]\sin(\theta)\cos^3(\theta) \\
&\quad \pm i[M_{x,\hat{\mathbf{p}}_x\perp\hat{\mathbf{n}}}(\mathbf{Q})M^*_{z,\hat{\mathbf{p}}_x\perp\hat{\mathbf{n}}}(\mathbf{Q}) \\
&\quad - M^*_{x,\hat{\mathbf{p}}_x\perp\hat{\mathbf{n}}}(\mathbf{Q})M_{z,\hat{\mathbf{p}}_x\perp\hat{\mathbf{n}}}(\mathbf{Q})]\sin(\theta)\cos(\theta) \\
&\quad \mp i[M_{y,\hat{\mathbf{p}}_x\perp\hat{\mathbf{n}}}(\mathbf{Q})M^*_{z,\hat{\mathbf{p}}_x\perp\hat{\mathbf{n}}}(\mathbf{Q}) - M^*_{y,\hat{\mathbf{p}}_x\perp\hat{\mathbf{n}}}(\mathbf{Q})M_{z,\hat{\mathbf{p}}_x\perp\hat{\mathbf{n}}}(\mathbf{Q})]\cos^2(\theta).
\end{aligned}$$
$$(6)$$

Similarly, the scattering from $\hat{\mathbf{p}} \parallel \hat{\mathbf{n}}$ derived using equations (3) and (4) becomes

$$\Upsilon_A(Q) = M_A,$$
$$\Upsilon_B(Q) = M_B \cos^2(\theta) - M_C \sin(\theta)\cos(\theta), \qquad (7)$$
$$\Upsilon_C(Q) = M_C \sin^2(\theta) - M_B \sin(\theta)\cos(\theta).$$

Recasting M_A, M_B and M_C as $M_{z,\hat{\mathbf{p}}_z\parallel\hat{\mathbf{n}}}$, $M_{x,\hat{\mathbf{p}}_z\parallel\hat{\mathbf{n}}}$ and $M_{y,\hat{\mathbf{p}}_z\parallel\hat{\mathbf{n}}}$, respectively, leads to

$$\begin{aligned}
\sigma^{\downarrow\downarrow}_{\uparrow\uparrow,\hat{\mathbf{p}}_z\parallel\hat{\mathbf{n}}}(\mathbf{Q}) &= N(\mathbf{Q})N^*(\mathbf{Q}) + M_{z,\hat{\mathbf{p}}_z\parallel\hat{\mathbf{n}}}(\mathbf{Q})M^*_{z,\hat{\mathbf{p}}_z\parallel\hat{\mathbf{n}}}(\mathbf{Q}) \\
&\quad \pm [M_{z,\hat{\mathbf{p}}_z\parallel\hat{\mathbf{n}}}(\mathbf{Q})(\theta)N^*(\mathbf{Q}) + M^*_{z,\hat{\mathbf{p}}_z\parallel\hat{\mathbf{n}}}(\mathbf{Q})N(\mathbf{Q})], \\
\sigma^{\uparrow\downarrow}_{\downarrow\uparrow,\hat{\mathbf{p}}_z\parallel\hat{\mathbf{n}}}(\mathbf{Q}) &= M_{x,\hat{\mathbf{p}}_z\parallel\hat{\mathbf{n}}}(\mathbf{Q})M^*_{x,\hat{\mathbf{p}}_z\parallel\hat{\mathbf{n}}}(\mathbf{Q})\sin^2(\theta) \\
&\quad + M_{y,\hat{\mathbf{p}}_z\parallel\hat{\mathbf{n}}}(\mathbf{Q})M^*_{y,\hat{\mathbf{p}}_z\parallel\hat{\mathbf{n}}}(\mathbf{Q})\cos^2(\theta) \\
&\quad - \sin(\theta)\cos(\theta)[M_{x,\hat{\mathbf{p}}_z\parallel\hat{\mathbf{n}}}(\mathbf{Q})M^*_{y,\hat{\mathbf{p}}_z\parallel\hat{\mathbf{n}}}(\mathbf{Q}) \\
&\quad + M^*_{x,\hat{\mathbf{p}}_z\parallel\hat{\mathbf{n}}}(\mathbf{Q})M_{y,\hat{\mathbf{p}}_z\parallel\hat{\mathbf{n}}}(\mathbf{Q})].
\end{aligned}$$
$$(8)$$

Table 1
Scattering terms for $\hat{\mathbf{p}} \perp \hat{\mathbf{n}}$ ($\mathbb{A}$, $\mathbb{B}$, $\mathbb{C}$ and $\mathbb{D}$) and $\hat{\mathbf{p}} \parallel \hat{\mathbf{n}}$ ($\mathbb{E}$, $\mathbb{F}$, $\mathbb{G}$ and $\mathbb{H}$).

Tag, operation	Result
$\mathbb{A}(\mathbf{Q}) = \sigma^{\downarrow\downarrow}_{\hat{\mathbf{p}}_x \perp \hat{\mathbf{n}}}(\mathbf{Q}) + \sigma^{\uparrow\uparrow}_{\hat{\mathbf{p}}_x \perp \hat{\mathbf{n}}}(\mathbf{Q})$	$\|N(\|\mathbf{Q}\|, \theta)\|^2 + \|M_{x,\hat{\mathbf{p}}_x \perp \hat{\mathbf{n}}}(\|\mathbf{Q}\|, \theta)\|^2 \sin^4(\theta) + \|M_{y,\hat{\mathbf{p}}_x \perp \hat{\mathbf{n}}}(\|\mathbf{Q}\|, \theta)\|^2 \cos^2(\theta)\sin^2(\theta) - 2\|M_{x,\hat{\mathbf{p}}_x \perp \hat{\mathbf{n}}}(\|\mathbf{Q}\|, \theta)\| \, \|M_{y,\hat{\mathbf{p}}_x \perp \hat{\mathbf{n}}}(\|\mathbf{Q}\|, \theta)\|$ $\times \overline{\cos}(\varphi_{M_x,\hat{\mathbf{p}}_x \perp \hat{\mathbf{n}}} - \varphi_{M_y,\hat{\mathbf{p}}_x \perp \hat{\mathbf{n}}}) \sin^3(\theta)\cos(\theta)$
$\mathbb{B}(\mathbf{Q}) = \sigma^{\downarrow\downarrow}_{\hat{\mathbf{p}}_x \perp \hat{\mathbf{n}}}(\mathbf{Q}) - \sigma^{\uparrow\uparrow}_{\hat{\mathbf{p}}_x \perp \hat{\mathbf{n}}}(\mathbf{Q})$	$2\|N(\|\mathbf{Q}\|, \theta)\| \, \|M_{x,\hat{\mathbf{p}}_x \perp \hat{\mathbf{n}}}(\|\mathbf{Q}\|, \theta)\| \, \overline{\cos}(\varphi_N - \varphi_{M_x,\hat{\mathbf{p}}_x \perp \hat{\mathbf{n}}}) \sin^2(\theta) - 2\|N(\|\mathbf{Q}\|, \theta)\| \, \|M_{y,\hat{\mathbf{p}}_x \perp \hat{\mathbf{n}}}(\|\mathbf{Q}\|, \theta)\| \, \overline{\cos}(\varphi_N - \varphi_{M_y,\hat{\mathbf{p}}_x \perp \hat{\mathbf{n}}}) \sin(\theta)\cos(\theta)$
$\mathbb{C}(\mathbf{Q}) = \sigma^{\uparrow\downarrow}_{\hat{\mathbf{p}}_x \perp \hat{\mathbf{n}}}(\mathbf{Q}) + \sigma^{\downarrow\uparrow}_{\hat{\mathbf{p}}_x \perp \hat{\mathbf{n}}}(\mathbf{Q})$	$\|M_{z,\hat{\mathbf{p}}_x \perp \hat{\mathbf{n}}}(\|\mathbf{Q}\|, \theta)\|^2 + \|M_{y,\hat{\mathbf{p}}_x \perp \hat{\mathbf{n}}}(\|\mathbf{Q}\|, \theta)\|^2 \cos^4(\theta) + \|M_{x,\hat{\mathbf{p}}_x \perp \hat{\mathbf{n}}}(\|\mathbf{Q}\|, \theta)\|^2 \sin^2(\theta)\cos^2(\theta) - 2\|M_{x,\hat{\mathbf{p}}_x \perp \hat{\mathbf{n}}}(\|\mathbf{Q}\|, \theta)\| \, \|M_{y,\hat{\mathbf{p}}_x \perp \hat{\mathbf{n}}}(\|\mathbf{Q}\|, \theta)\|$ $\times \overline{\cos}(\varphi_{M_x,\hat{\mathbf{p}}_x \perp \hat{\mathbf{n}}} - \varphi_{M_y,\hat{\mathbf{p}}_x \perp \hat{\mathbf{n}}}) \sin(\theta)\cos^3(\theta)$
$\mathbb{D}(\mathbf{Q}) = \sigma^{\uparrow\downarrow}_{\hat{\mathbf{p}}_x \perp \hat{\mathbf{n}}}(\mathbf{Q}) - \sigma^{\downarrow\uparrow}_{\hat{\mathbf{p}}_x \perp \hat{\mathbf{n}}}(\mathbf{Q})$	$2\|M_{y,\hat{\mathbf{p}}_x \perp \hat{\mathbf{n}}}(\|\mathbf{Q}\|, \theta)\| \, \|M_{z,\hat{\mathbf{p}}_x \perp \hat{\mathbf{n}}}(\|\mathbf{Q}\|, \theta)\| \, \overline{\sin}(\varphi_{M_y,\hat{\mathbf{p}}_x \perp \hat{\mathbf{n}}} - \varphi_{M_z,\hat{\mathbf{p}}_x \perp \hat{\mathbf{n}}}) \cos^2(\theta) - 2\|M_{x,\hat{\mathbf{p}}_x \perp \hat{\mathbf{n}}}(\|\mathbf{Q}\|, \theta)\| \, \|M_{z,\hat{\mathbf{p}}_x \perp \hat{\mathbf{n}}}(\|\mathbf{Q}\|, \theta)\|$ $\times \overline{\sin}(\varphi_{M_x,\hat{\mathbf{p}}_x \perp \hat{\mathbf{n}}} - \varphi_{M_z,\hat{\mathbf{p}}_x \perp \hat{\mathbf{n}}}) \sin(\theta)\cos(\theta)$
$\mathbb{E}(\mathbf{Q}) = \sigma^{\downarrow\downarrow}_{\hat{\mathbf{p}}_z \parallel \hat{\mathbf{n}}}(\mathbf{Q}) + \sigma^{\uparrow\uparrow}_{\hat{\mathbf{p}}_z \parallel \hat{\mathbf{n}}}(\mathbf{Q})$	$\|N(\|\mathbf{Q}\|, \theta)\|^2 + \|M_{z,\hat{\mathbf{p}}_z \parallel \hat{\mathbf{n}}}(\|\mathbf{Q}\|, \theta)\|^2$
$\mathbb{F}(\mathbf{Q}) = \sigma^{\downarrow\downarrow}_{\hat{\mathbf{p}}_z \parallel \hat{\mathbf{n}}}(\mathbf{Q}) - \sigma^{\uparrow\uparrow}_{\hat{\mathbf{p}}_z \parallel \hat{\mathbf{n}}}(\mathbf{Q})$	$2\|N(\|\mathbf{Q}\|, \theta)\| \, \|M_{z,\hat{\mathbf{p}}_z \parallel \hat{\mathbf{n}}}(\|\mathbf{Q}\|, \theta)\| \, \overline{\cos}(\varphi_N - \varphi_{M_z,\hat{\mathbf{p}}_z \parallel \hat{\mathbf{n}}})$
$\mathbb{G}(\mathbf{Q}) = \sigma^{\uparrow\downarrow}_{\hat{\mathbf{p}}_z \parallel \hat{\mathbf{n}}}(\mathbf{Q}) + \sigma^{\downarrow\uparrow}_{\hat{\mathbf{p}}_z \parallel \hat{\mathbf{n}}}(\mathbf{Q})$	$\|M_{x,\hat{\mathbf{p}}_z \parallel \hat{\mathbf{n}}}(\|\mathbf{Q}\|, \theta)\|^2 \sin^2(\theta) + \|M_{y,\hat{\mathbf{p}}_z \parallel \hat{\mathbf{n}}}(\|\mathbf{Q}\|, \theta)\|^2 \cos^2(\theta) - 2\|M_{x,\hat{\mathbf{p}}_z \parallel \hat{\mathbf{n}}}(\|\mathbf{Q}\|, \theta)\| \, \|M_{y,\hat{\mathbf{p}}_z \parallel \hat{\mathbf{n}}}(\|\mathbf{Q}\|, \theta)\| \, \overline{\cos}(\varphi_{M_x,\hat{\mathbf{p}}_z \parallel \hat{\mathbf{n}}} - \varphi_{M_y,\hat{\mathbf{p}}_z \parallel \hat{\mathbf{n}}}) \sin(\theta)\cos(\theta)$
$\mathbb{H}(\mathbf{Q}) = \sigma^{\uparrow\downarrow}_{\hat{\mathbf{p}}_z \parallel \hat{\mathbf{n}}}(\mathbf{Q}) - \sigma^{\downarrow\uparrow}_{\hat{\mathbf{p}}_z \parallel \hat{\mathbf{n}}}(\mathbf{Q})$	0

Table 2
Angular scattering dependence for structural and magnetic isotropic samples.

$\mathbb{A}$, $\mathbb{C}$, $\mathbb{E}$ and $\mathbb{G}$ are defined in Table 1. The sign of terms containing odd numbers of $\sin(\theta)$ and $\cos(\theta)$ may oscillate.

Terms for $\hat{\mathbf{p}} \perp \hat{\mathbf{n}}$.

	$\mathbb{A}$	$\mathbb{B}$	$\mathbb{C}$	Unpol ($\mathbb{A} + \mathbb{C}$)
$\|N\|^2$	1	0	0	1
$\|M_x\|^2$	$\sin^4(\theta)$	0	$\sin^2(\theta)\cos^2(\theta)$	$\sin^2(\theta)$
$\|M_y\|^2$	$\sin^2(\theta)\cos^2(\theta)$	0	$\cos^4(\theta)$	$\cos^2(\theta)$
$\|M_z\|^2$	0	0	1	1
$2\|N\|\,\|M_x\|\,\overline{\cos}(\varphi_N - \varphi_{M_x})$	0	1	0	0
$-2\|N\|\,\|M_y\|\,\overline{\cos}(\varphi_N - \varphi_{M_y})$	0	1	0	0
$-2\|M_x\|\,\|M_y\|\,\overline{\cos}(\varphi_{M_x} - \varphi_{M_y})$	$\sin^3(\theta)\cos(\theta)$	0	$\sin(\theta)\cos^3(\theta)$	$\sin(\theta)\cos(\theta)$

Terms for $\hat{\mathbf{p}} \parallel \hat{\mathbf{n}}$. The choice of X and Y axes within the plane $\perp \hat{\mathbf{n}}$ is arbitrary.

	$\mathbb{E}$	$\mathbb{F}$	$\mathbb{G}$	Unpol ($\mathbb{E} + \mathbb{G}$)
$\|N\|^2$	1	0	0	1
$\|M_z\|^2$	1	0	0	1
$\|M_x\|^2$	0	0	$\sin^2(\theta)$	$\sin^2(\theta)$
$\|M_y\|^2$	0	0	$\cos^2(\theta)$	$\cos^2(\theta)$
$2\|N\|\,\|M_z\|\,\overline{\cos}(\varphi_N - \varphi_{M_z})$	0	1	0	0
$-2\|M_x\|\,\|M_y\|\,\overline{\cos}(\varphi_{M_x} - \varphi_{M_y})$	0	0	$\sin(\theta)\cos(\theta)$	$\sin(\theta)\cos(\theta)$

In simplifying equations (6) and (8) the scattering transform of $N, M_J(\mathbf{Q})$, equation (1), can be written more succinctly (Brown, 2001) in terms of an amplitude, $\|N, M_J\| \equiv (\text{Re}\|N, M_J\|^2 + \text{Im}\|N, M_J\|^2)^{1/2}$, and a net phase, φ_{N,M_J}, as

$$N, M_J(\mathbf{Q}) = \|N, M_J\| \exp(i\varphi_{N,M_J}). \quad (9)$$

If α and β represent non-equivalent terms of $N, M_J(\mathbf{Q})$, then

$$\alpha\alpha^* = \|\alpha\|^2,$$
$$\alpha\beta^* + \alpha^*\beta = 2\|\alpha\|\,\|\beta\|\,\overline{\cos}(\varphi_\alpha - \varphi_\beta), \quad (10)$$
$$i(\alpha\beta^* - \alpha^*\beta) = -2\|\alpha\|\,\|\beta\|\,\overline{\sin}(\varphi_\alpha - \varphi_\beta).$$

Here, $\|\alpha\|^2$ represents the intensity measured from one type of scatterer (*i.e.* structural scattering or scattering from the

projection of magnetic moments oriented along a particular axis). Combinations of α and β can be positive or negative and are referred to as interference terms. The averaging of the sines and cosines ($\overline{\sin}$ and $\overline{\cos}$) is used as a reminder that each scattering neutron has a spatial coherence length smaller than that of the macroscopic sample and, thus, α and β each represent a sum of scattering amplitudes. Note that the sine and cosine terms involve only the difference between φ values from these scattering components, and the absolute value of each φ is immaterial. Therefore, an interference term is only nonzero if there is a preserved phase difference that does not average out across the sample. If $\overline{\cos}(\varphi_\alpha - \varphi_\beta) = \pm 1$ or 0, then α and β are said to be in-phase and out-of-phase, respectively. Table 1 defines reduced forms of the scattering cross sections obtained from equations (6) and (8) that will be demonstrated to be useful (see §6 below) in isolating the structural and individual magnetic scattering components from the θ and $\mathbf{Q}$ symmetry of the scattering.

In the case of a sample in which the structural and individual magnetic components are each spatially isotropic, the relative contribution from each component can be identified by considering the angular dependence of the reduced terms defined in Table 1. These simple symmetries are provided in Table 2 for $\hat{\mathbf{p}} \perp \hat{\mathbf{n}}$, $\hat{\mathbf{p}} \parallel \hat{\mathbf{n}}$ and unpolarized (Unpol) experiments. Simultaneous fitting for all scattering components as a function of θ has been successfully employed to yield highly detailed magnetic information (Wiedenmann, 2005; Michels & Weissmüller, 2008; Dufour *et al.*, 2011). However, one must be very careful in performing this angular analysis (as will be shown in the next section) since the sign of the terms containing odd numbers of $\cos(\theta)$ and $\sin(\theta)$ may or may not oscillate sign with quadrant, depending entirely upon the magnetic symmetry of the sample.

5. Interference terms and symmetry

$\mathbb{A}$, $\mathbb{B}$, $\mathbb{C}$, $\mathbb{D}$, $\mathbb{F}$ and $\mathbb{G}$ (defined in Table 1) all contain interference terms and, as such, it would be advantageous to be

able to separate them further on the basis of angular symmetry (*i.e.* comparison of $+\theta$ and $-\theta$ scattering) for the majority of samples whose structural morphology is spatially symmetric with respect to $\hat{\mathbf{p}}$. Naively the interference terms of Table 1 that contain an odd number of $\sin(\theta)$ and $\cos(\theta)$ terms would be expected to oscillate in sign with quadrant, while those containing an even number of $\sin(\theta)$ and $\cos(\theta)$ terms would not. Before fully utilizing $\pm\theta$ scattering comparisons, however, we need a solid understanding of how the terms of the form $|\alpha|\,|\beta|\,\overline{\sin}(\varphi_\beta - \varphi_\alpha)$ and $|\alpha|\,|\beta|\,\overline{\cos}(\varphi_\beta - \varphi_\alpha)$ may also change sign as a function of quadrant.

To illustrate this, let us examine the interference term $-2|M_{x,\hat{\mathbf{p}}_x\perp\hat{\mathbf{n}}}(|\mathbf{Q}|,\theta)|\,|M_{y,\hat{\mathbf{p}}_x\perp\hat{\mathbf{n}}}(|\mathbf{Q}|,\theta)|\,\overline{\cos}(\varphi_{M_x,\hat{\mathbf{p}}_x\perp\hat{\mathbf{n}}} - \varphi_{M_y,\hat{\mathbf{p}}_x\perp\hat{\mathbf{n}}}) \times \sin^m(\theta)\cos^n(\theta)$ [*i.e.* $\mathbb{A}(\mathbf{Q})$ and $\mathbb{C}(\mathbf{Q})$ in Table 1], where n and m are odd integers. The results from simulations for a series of basic magnetic morphologies are shown in Fig. 2, where each box corresponds to a scattering unit with $\rho_N = 1$ and $\rho_M = 1$, pointing in the direction shown, or $\rho_M = 0$ where no arrow is shown. From Fig. 2 it becomes evident that closed-domain structures with zero net moment (structures v, vi, vii), of either chirality or a mix of chiral sub-units, contribute positively in all quadrants with maxima at $\theta = 45, 135, 225$ and $315°$. This is akin to the fourfold symmetry of dipolar structures reported by Michels & Weissmüller (2008), and such scattering underscores that, even if there is no net magnetic moment, a prominent scattering contribution can be observed if there is a magnetic modulation along $\mathbf{Q}$.

Structures with a net moment along the X axis, but not along the Y axis (structures iii and iv), may contribute positively or negatively in each quadrant, but the scattering will be the same for $\pm\theta$. Similarly, structures with a net moment along the Y axis, but not along the X axis (*i.e.* structures iii or iv rotated by $90°$), may again contribute positively or negatively in each quadrant, with scattering of the same sign for $\pm\theta$. However, if there is a net moment along the X axis and a net moment along the Y axis (as in a unidirectional magnetic

domain, structures i and ii), then the resulting scattering contributions oscillate sign with quadrant. Notice that for structures containing a net moment (i through iv) the sign of $\overline{\cos}(\varphi_{M_x,\hat{\mathbf{p}}_x\perp\hat{\mathbf{n}}} - \varphi_{M_y,\hat{\mathbf{p}}_x\perp\hat{\mathbf{n}}})$ flips when comparing two structures in which either the X or the Y orientation of the moments is reversed, but the sign remains unaltered when comparing two structures in which both the X and the Y orientations of the moments are reversed. In summary, a scattering difference between $-\theta$ and $+\theta$ can arise from a nonzero $-2|M_{x,\hat{\mathbf{p}}_x\perp\hat{\mathbf{n}}}(|\mathbf{Q}|,\theta)|\,|M_{y,\hat{\mathbf{p}}_x\perp\hat{\mathbf{n}}}(|\mathbf{Q}|,\theta)|\,\overline{\cos}(\varphi_{M_x,\hat{\mathbf{p}}_x\perp\hat{\mathbf{n}}} - \varphi_{M_y,\hat{\mathbf{p}}_x\perp\hat{\mathbf{n}}}) \times \sin^m(\theta)\cos^n(\theta)$ term if there is a net moment along the X axis and also a net moment along the Y axis (*i.e.* if there exists a net canted moment that does not average to zero across the sample).

The simulations shown in Fig. 2 can be used as well to understand the interference between $N(\mathbf{Q})$ and $M(\mathbf{Q})$, where $N(\mathbf{Q})$ is equivalent in angular symmetry to an $M(\mathbf{Q})$ of positive net moment. This implies that nuclear–magnetic interferences similar to i through iv could exist, but not structures v through vii, as the sign (direction) of $N(\mathbf{Q})$ cannot change. Thus, $-2|N(|\mathbf{Q}|,\theta)|\,|M_{y,\hat{\mathbf{p}}_x\perp\hat{\mathbf{n}}}(|\mathbf{Q}|,\theta)|\,\overline{\cos}(\varphi_N - \varphi_{M_y,\hat{\mathbf{p}}_x\perp\hat{\mathbf{n}}})\sin(\theta)\cos(\theta)$ (from $\mathbb{B}$ in Table 1) will oscillate sign with quadrant if there is a net moment along the Y axis, but it will exhibit a uniform sign for all quadrants if there are magnetic modulations without a net $M_{y,\hat{\mathbf{p}}_x\perp\hat{\mathbf{n}}}(|\mathbf{Q}|,\theta)$ moment. Conversely, $2|N(|\mathbf{Q}|,\theta)| \times |M_{x,\hat{\mathbf{p}}_x\perp\hat{\mathbf{n}}}(|\mathbf{Q}|,\theta)|\,\overline{\cos}(\varphi_N - \varphi_{M_x,\hat{\mathbf{p}}_x\perp\hat{\mathbf{n}}})\sin^2(\theta)$ (from $\mathbb{B}$ in Table 1) and $2|N(|\mathbf{Q}|,\theta)|\,|M_{z,\hat{\mathbf{p}}_z\|\hat{\mathbf{n}}}(|\mathbf{Q}|,\theta)|\,\overline{\cos}(\varphi_N - \varphi_{M_z,\hat{\mathbf{p}}_z\|\hat{\mathbf{n}}})$ (from $\mathbb{F}$ in Table 1), which do not contain oscillating $\sin^m(\theta)\cos^n(\theta)$ terms, would be expected to be positive in all quadrants for a net magnetic moment aligned parallel to the positive X or Y axis, respectively. Notice how structures iii and iv in Fig. 2, which are similar in pattern but have different domain edge locations, cancel when added together. Combining this long-range isomorphism between $N(\mathbf{Q})$ and $M(\mathbf{Q})$, which is needed for a strong nuclear–magnetic interference term to exist, it becomes highly probable that any nuclear–magnetic interference term observed will originate only from net $M_{x,\hat{\mathbf{p}}_x\perp\hat{\mathbf{n}}}(|\mathbf{Q}|,\theta)$ or net $M_{y,\hat{\mathbf{p}}_x\perp\hat{\mathbf{n}}}(|\mathbf{Q}|,\theta)$ moments. To identify these nuclear–magnetic ($\mathbb{B}'$ and $\mathbb{B}''$) and magnetic–magnetic ($\mathbb{A}'$ and $\mathbb{A}''$, $\mathbb{C}'$ and $\mathbb{C}''$, or $\mathbb{G}'$ and $\mathbb{G}''$) correlations in the experimental data, it is essential to isolate interference terms by comparing $\pm\theta$ scattering as shown in Table 3.

The remaining interference terms (both from $\mathbb{D}$ in Table 1), $-2|M_{y,\hat{\mathbf{p}}_x\perp\hat{\mathbf{n}}}(|\mathbf{Q}|,\theta)|\,|M_{z,\hat{\mathbf{p}}_x\perp\hat{\mathbf{n}}}(|\mathbf{Q}|,\theta)|\,\overline{\sin}(\varphi_{M_y,\hat{\mathbf{p}}_x\perp\hat{\mathbf{n}}} - \varphi_{M_z,\hat{\mathbf{p}}_x\perp\hat{\mathbf{n}}}) \times \cos^2(\theta)$ and $2|M_{x,\hat{\mathbf{p}}_x\perp\hat{\mathbf{n}}}(|\mathbf{Q}|,\theta)|\,|M_{z,\hat{\mathbf{p}}_x\perp\hat{\mathbf{n}}}(|\mathbf{Q}|,\theta)|\,\overline{\sin}(\varphi_{M_x,\hat{\mathbf{p}}_x\perp\hat{\mathbf{n}}} - \varphi_{M_z,\hat{\mathbf{p}}_x\perp\hat{\mathbf{n}}})\sin(\theta)\cos(\theta)$, are observable as a difference in spin-flip scattering. They are different from the other interferences in that there is a sine, rather than cosine, dependence to their phase differences. Thus, unlike the previous interferences discussed for which there is a maximum when the interfering terms are in phase, these interferences disappear when the phase difference approaches zero. Instead, they become nonzero only when there is a net phase difference preserved across the sample, which would be indicative of an underlying magnetic chiral structure. While previous research (Brown, 2001; Maleyev, 2004; Schweika, 2010) has shown that a nonzero difference in the spin-flip scattering at $\theta = 0°$ is key to
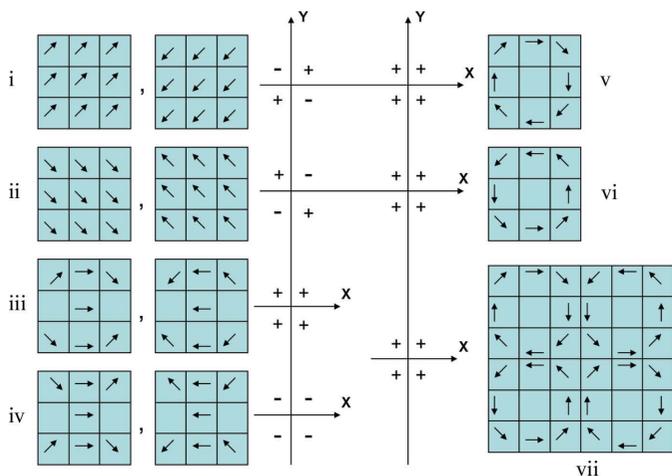
Figure 2
The scattering symmetry of $-2|M_{x,\hat{\mathbf{p}}_x\perp\hat{\mathbf{n}}}(|\mathbf{Q}|,\theta)|\,|M_{y,\hat{\mathbf{p}}_x\perp\hat{\mathbf{n}}}(|\mathbf{Q}|,\theta)| \times \overline{\cos}(\varphi_{M_x,\hat{\mathbf{p}}_x\perp\hat{\mathbf{n}}} - \varphi_{M_y,\hat{\mathbf{p}}_x\perp\hat{\mathbf{n}}})\sin^m(\theta)\cos^n(\theta)$, for odd m and n, is shown for a series of basic magnetic morphologies. Although the absolute sign may vary, the relative change of sign as a function of quadrant is key.

Table 3
Reduction *via* symmetry considerations.

Tag, operation	Result
$\mathbb{A}'(|\mathbf{Q}|, \theta) = \frac{1}{2}[\mathbb{A}(|\mathbf{Q}|, \theta) + \mathbb{A}(|\mathbf{Q}|, -\theta)]$	$|N(|\mathbf{Q}|, \theta)|^2 + |M_{x,\hat{\mathbf{p}}_x\perp\hat{\mathbf{n}}}(|\mathbf{Q}|, \theta)|^2 \sin^4(\theta) + |M_{y,\hat{\mathbf{p}}_x\perp\hat{\mathbf{n}}}(|\mathbf{Q}|, \theta)|^2 \cos^2(\theta)\sin^2(\theta)$
	Add $-2|M_{x,\hat{\mathbf{p}}_x\perp\hat{\mathbf{n}}}(|\mathbf{Q}|, \theta)||M_{y,\hat{\mathbf{p}}_x\perp\hat{\mathbf{n}}}(|\mathbf{Q}|, \theta)|\overline{\cos}(\varphi_{M_x,\hat{\mathbf{p}}_x\perp\hat{\mathbf{n}}} - \varphi_{M_y,\hat{\mathbf{p}}_x\perp\hat{\mathbf{n}}})\sin^3(\theta)\cos(\theta)$ if net M_x, net M_y or closed $M_x M_y$ domains
$\mathbb{A}''(|\mathbf{Q}|, \theta) = \frac{1}{2}[\mathbb{A}(|\mathbf{Q}|, \theta) - \mathbb{A}(|\mathbf{Q}|, -\theta)]$	$-2|M_{x,\hat{\mathbf{p}}_x\perp\hat{\mathbf{n}}}(|\mathbf{Q}|, \theta)||M_{y,\hat{\mathbf{p}}_x\perp\hat{\mathbf{n}}}(|\mathbf{Q}|, \theta)|\overline{\cos}(\varphi_{M_x,\hat{\mathbf{p}}_x\perp\hat{\mathbf{n}}} - \varphi_{M_y,\hat{\mathbf{p}}_x\perp\hat{\mathbf{n}}})\sin^3(\theta)\cos(\theta)$ if net M_x and net M_y moments
$\mathbb{B}'(|\mathbf{Q}|, \theta) = \frac{1}{2}[\mathbb{B}(|\mathbf{Q}|, \theta) + \mathbb{B}(|\mathbf{Q}|, -\theta)]$	$2|N(|\mathbf{Q}|, \theta)||M_{x,\hat{\mathbf{p}}_x\perp\hat{\mathbf{n}}}(|\mathbf{Q}|, \theta)|\overline{\cos}(\varphi_N - \varphi_{M_x,\hat{\mathbf{p}}_x\perp\hat{\mathbf{n}}})\sin^2(\theta)$ if net M_x
	May also observe $-2|N(|\mathbf{Q}|, \theta)||M_{y,\hat{\mathbf{p}}_x\perp\hat{\mathbf{n}}}(|\mathbf{Q}|, \theta)|\overline{\cos}(\varphi_N - \varphi_{M_x,\hat{\mathbf{p}}_x\perp\hat{\mathbf{n}}})\sin(\theta)\cos(\theta)$ if zero sum, but spatially modulated M_y
$\mathbb{B}''(|\mathbf{Q}|, \theta) = \frac{1}{2}[\mathbb{B}(|\mathbf{Q}|, \theta) - \mathbb{B}(|\mathbf{Q}|, -\theta)]$	$-2|N(|\mathbf{Q}|, \theta)||M_{y,\hat{\mathbf{p}}_x\perp\hat{\mathbf{n}}}(|\mathbf{Q}|, \theta)|\overline{\cos}(\varphi_N - \varphi_{M_x,\hat{\mathbf{p}}_x\perp\hat{\mathbf{n}}})\sin(\theta)\cos(\theta)$ if net M_y
	May also observe $2|N(|\mathbf{Q}|, \theta)||M_{x,\hat{\mathbf{p}}_x\perp\hat{\mathbf{n}}}(|\mathbf{Q}|, \theta)|\overline{\cos}(\varphi_N - \varphi_{M_x,\hat{\mathbf{p}}_x\perp\hat{\mathbf{n}}})\sin^2(\theta)$ if zero sum, but spatially modulated M_x
$\mathbb{C}'(|\mathbf{Q}|, \theta) = \frac{1}{2}[\mathbb{C}(|\mathbf{Q}|, \theta) + \mathbb{C}(|\mathbf{Q}|, -\theta)]$	$|M_{z,\hat{\mathbf{p}}_x\perp\hat{\mathbf{n}}}(|\mathbf{Q}|, \theta)|^2 + |M_{y,\hat{\mathbf{p}}_x\perp\hat{\mathbf{n}}}(|\mathbf{Q}|, \theta)|^2 \cos^4(\theta) + |M_{z,\hat{\mathbf{p}}_x\perp\hat{\mathbf{n}}}(|\mathbf{Q}|, \theta)|^2 \sin^2(\theta)\cos^2(\theta)$
	Add $-2|M_{x,\hat{\mathbf{p}}_x\perp\hat{\mathbf{n}}}(|\mathbf{Q}|, \theta)||M_{y,\hat{\mathbf{p}}_x\perp\hat{\mathbf{n}}}(|\mathbf{Q}|, \theta)|\overline{\cos}(\varphi_{M_x,\hat{\mathbf{p}}_x\perp\hat{\mathbf{n}}} - \varphi_{M_y,\hat{\mathbf{p}}_x\perp\hat{\mathbf{n}}})\sin(\theta)\cos^3(\theta)$ if net M_x, net M_y or closed $M_x M_y$ domains
$\mathbb{C}''(|\mathbf{Q}|, \theta) = \frac{1}{2}[\mathbb{C}(|\mathbf{Q}|, \theta) - \mathbb{C}(|\mathbf{Q}|, -\theta)]$	$-2|M_{x,\hat{\mathbf{p}}_x\perp\hat{\mathbf{n}}}(|\mathbf{Q}|, \theta)||M_{y,\hat{\mathbf{p}}_x\perp\hat{\mathbf{n}}}(|\mathbf{Q}|, \theta)|\overline{\cos}(\varphi_{M_x,\hat{\mathbf{p}}_x\perp\hat{\mathbf{n}}} - \varphi_{M_y,\hat{\mathbf{p}}_x\perp\hat{\mathbf{n}}})\sin(\theta)\cos^3(\theta)$ if net M_x and net M_y moments
$\mathbb{G}'(|\mathbf{Q}|, \theta) = \frac{1}{2}[\mathbb{G}(|\mathbf{Q}|, \theta) + \mathbb{G}(|\mathbf{Q}|, -\theta)]$	$|M_{x,\hat{\mathbf{p}}_z\|\hat{\mathbf{n}}}(|\mathbf{Q}|, \theta)|^2 \sin^2(\theta) + |M_{y,\hat{\mathbf{p}}_z\|\hat{\mathbf{n}}}(|\mathbf{Q}|, \theta)|^2 \cos^2(\theta)$
	Add $-2|M_{x,\hat{\mathbf{p}}_z\|\hat{\mathbf{n}}}(|\mathbf{Q}|, \theta)||M_{y,\hat{\mathbf{p}}_z\|\hat{\mathbf{n}}}(|\mathbf{Q}|, \theta)|\overline{\cos}(\varphi_{M_x,\hat{\mathbf{p}}_z\|\hat{\mathbf{n}}} - \varphi_{M_y,\hat{\mathbf{p}}_z\|\hat{\mathbf{n}}})\sin(\theta)\cos(\theta)$ if M_x, net M_y or closed $M_x M_y$ domains
$\mathbb{G}''(|\mathbf{Q}|, \theta) = \frac{1}{2}[\mathbb{G}(|\mathbf{Q}|, \theta) - \mathbb{G}(|\mathbf{Q}|, -\theta)]$	$-2|M_{x,\hat{\mathbf{p}}_z\|\hat{\mathbf{n}}}(|\mathbf{Q}|, \theta)||M_{y,\hat{\mathbf{p}}_z\|\hat{\mathbf{n}}}(|\mathbf{Q}|, \theta)|\overline{\cos}(\varphi_{M_x,\hat{\mathbf{p}}_z\|\hat{\mathbf{n}}} - \varphi_{M_y,\hat{\mathbf{p}}_z\|\hat{\mathbf{n}}})\sin(\theta)\cos(\theta)$ if net M_x, net M_y moments

identifying chiral structures, the θ dependence of this difference can reveal the components of magnetization [$M_{z,\hat{\mathbf{p}}_x\perp\hat{\mathbf{n}}}(\mathbf{Q})$ and $M_{x,\hat{\mathbf{p}}_x\perp\hat{\mathbf{n}}}(\mathbf{Q})$ or $M_{z,\hat{\mathbf{p}}_x\perp\hat{\mathbf{n}}}(\mathbf{Q})$ and $M_{y,\hat{\mathbf{p}}_x\perp\hat{\mathbf{n}}}(\mathbf{Q})$] that participate in the spin spiral.

6. General cases for nuclear and magnetic separation

Assorted constraints regarding structural uniformity, the relative strengths of the magnetic moments oriented in specific directions or the correlation between scattering terms may be applied to simplify further the scattering equations given in Tables 1 and 3 in order to isolate the structural and magnetic components. In the remaining part of this paper we describe some commonly encountered cases, their reduced scattering equations and the specific requirements that must be met for usage. The results are summarized in Table 4. Let us begin with the most general conditions in which one has no knowledge of sample isotropy or the relative behavior of the magnetic components.

6.1. Case 1: general $\hat{\mathbf{p}} \| \hat{\mathbf{n}}$

For $\hat{\mathbf{p}} \| \hat{\mathbf{n}}$, equation (8) reduces to

$$|N(\mathbf{Q})|^2 + |M_{z,\hat{\mathbf{p}}_z\|\hat{\mathbf{n}}}(\mathbf{Q})|^2 = \mathbb{E}(\mathbf{Q}),$$
$$|M_{x,\hat{\mathbf{p}}_z\|\hat{\mathbf{n}}}(|\mathbf{Q}|, 90°)|^2 = \mathbb{G}(|\mathbf{Q}|, 90°), \qquad (11)$$
$$|M_{y,\hat{\mathbf{p}}_z\|\hat{\mathbf{n}}}(|\mathbf{Q}|, 0°)|^2 = \mathbb{G}(|\mathbf{Q}|, 0°).$$

The interference term between $M_{x,\hat{\mathbf{p}}_z\|\hat{\mathbf{n}}}(\mathbf{Q})$ and $M_{y,\hat{\mathbf{p}}_z\|\hat{\mathbf{n}}}(\mathbf{Q})$ vanishes at $\theta = 0$ and $90°$, yet the original choice of the X and Y axes is arbitrary within the $\hat{\mathbf{p}} \| \hat{\mathbf{n}}$ geometry. The underlying mathematics does not preclude the existence of interference terms arising from moments that are linear combinations of $M_{x,\hat{\mathbf{p}}_z\|\hat{\mathbf{n}}}(\mathbf{Q})$ and $M_{y,\hat{\mathbf{p}}_z\|\hat{\mathbf{n}}}(\mathbf{Q})$. Thus, it is more general to express

$\mathbb{G}(\mathbf{Q})$ in terms of a net magnetic moment that is both $\perp \mathbf{Q}$ and $\perp \hat{\mathbf{n}}$, namely $M_{\theta\pm90°,\hat{\mathbf{p}}_z\|\hat{\mathbf{n}}}(\mathbf{Q})$, plus an interference that arises from the projection of magnetic moments, namely $M_{\theta+45°,\hat{\mathbf{p}}_z\|\hat{\mathbf{n}}}(\mathbf{Q})$ and $M_{\theta-45°,\hat{\mathbf{p}}_z\|\hat{\mathbf{n}}}(\mathbf{Q})$, onto coordinates axes which are defined to be $\perp \hat{\mathbf{n}}$ and located at $\theta + 45°$ and $\theta - 45°$, respectively. Thus (Case 1, Table 4),

$$|M_{\theta\pm90°,\hat{\mathbf{p}}_z\|\hat{\mathbf{n}}}(\mathbf{Q})|^2 - |M_{\theta+45°,\hat{\mathbf{p}}_z\|\hat{\mathbf{n}}}(|\mathbf{Q}|, \theta)||M_{\theta-45°,\hat{\mathbf{p}}_z\|\hat{\mathbf{n}}}(|\mathbf{Q}|, \theta)|$$
$$\times \overline{\cos}(\varphi_{M_{\theta+45°},\hat{\mathbf{p}}_z\|\hat{\mathbf{n}}} - \varphi_{M_{\theta-45°},\hat{\mathbf{p}}_z\|\hat{\mathbf{n}}}) = \mathbb{G}(\mathbf{Q}). \quad (12)$$

This representation is distinct from previous descriptions in that the defined directions of measured magnetism rotate with $\mathbf{Q}$. This geometry is ideal for measuring magnetic moments $\perp \hat{\mathbf{p}}$ if there is no interference between $M_{\theta+45°,\hat{\mathbf{p}}_z\|\hat{\mathbf{n}}}(|\mathbf{Q}|, \theta)$ and $M_{\theta-45°,\hat{\mathbf{p}}_z\|\hat{\mathbf{n}}}(|\mathbf{Q}|, \theta)$. However, equation (12) would tend toward zero if the interference term were sufficiently strong, complicating the extraction of $|M_{\theta\pm90°,\hat{\mathbf{p}}_z\|\hat{\mathbf{n}}}(\mathbf{Q})|^2$. It is also difficult to separate $|N(\mathbf{Q})|^2$ from $|M_{z,\hat{\mathbf{p}}_x\perp\hat{\mathbf{n}}}(\mathbf{Q})|^2$ from $\mathbb{E}$ (Table 1) alone.

6.2. Case 2: N and M_X in phase for $\hat{\mathbf{p}} \| \hat{\mathbf{n}}$

However, if it were known that $|N(\mathbf{Q})|^2$ and $|M_{z,\hat{\mathbf{p}}_x\perp\hat{\mathbf{n}}}(\mathbf{Q})|^2$ were fully in phase [*i.e.* $|\overline{\cos}(\varphi_N - \varphi_{M_z,\hat{\mathbf{p}}_z\|\hat{\mathbf{n}}})| \Rightarrow 1$, where the long-range nuclear and magnetic morphologies share the same structure factors, as is typical under conditions of magnetic saturation], then it would be possible to separate these terms (Case 2, Table 4) using

$$|N(\mathbf{Q})|^2, |M_{z,\hat{\mathbf{p}}_z\|\hat{\mathbf{n}}}(\mathbf{Q})|^2 = \frac{1}{2}\left\{\mathbb{E}(\mathbf{Q}) \pm \left[\mathbb{E}^2(\mathbf{Q}) - \mathbb{F}^2(\mathbf{Q})\right]^{1/2}\right\}, \quad (13)$$

where the larger of the two terms [usually $|N(\mathbf{Q})|^2$] corresponds to the positive root. If additionally the structure is known to be independent of the applied field, then it would be reasonable to use $|N(\mathbf{Q})|^2$ obtained from equation (13) at saturation as input for equation (11) in order to extract

Kathryn Krycka *et al.* · PASANS. II. Mathematical angular analysis

Table 4
Four cross-section analysis procedures.

The condition of $|\overline{\cos}(\varphi_1 - \varphi_2)| \Rightarrow 1$ implies that the constituent terms are in phase. General cases 1 and 3 are not repeated, but can be used for every $\hat{\mathbf{p}} \parallel \hat{\mathbf{n}}$ or $\hat{\mathbf{p}} \perp \hat{\mathbf{n}}$ situation, respectively. $\beta(\mathbf{Q})$ is defined in the text.

Case	Requirements for $\hat{\mathbf{p}}_z \parallel \hat{\mathbf{n}}$	Equations
1	None	$|N(\mathbf{Q})|^2 + |M_{z,\hat{\mathbf{p}}_z\|\hat{\mathbf{n}}}(\mathbf{Q})|^2 = \mathbb{E}(\mathbf{Q})$
		$|M_{\theta\pm90°,\hat{\mathbf{p}}_z\|\hat{\mathbf{n}}}(\mathbf{Q})|^2 - |M_{\theta+45°,\hat{\mathbf{p}}_z\|\hat{\mathbf{n}}}(\mathbf{Q})|\,|M_{\theta-45°,\hat{\mathbf{p}}_z\|\hat{\mathbf{n}}}(\mathbf{Q})|\,\overline{\cos}(\varphi_{M_{\theta+45°},\hat{\mathbf{p}}_z\|\hat{\mathbf{n}}} - \varphi_{M_{\theta-45°},\hat{\mathbf{p}}_z\|\hat{\mathbf{n}}}) = \mathbb{G}(\mathbf{Q})$
2	$|\overline{\cos}(\varphi_N - \varphi_{M_z,\hat{\mathbf{p}}_z\|\hat{\mathbf{n}}})| \Rightarrow 1$	$|N(\mathbf{Q})|^2, |M_{z,\hat{\mathbf{p}}_z\|\hat{\mathbf{n}}}(\mathbf{Q})|^2 = \frac{1}{2}\{\mathbb{E}(\mathbf{Q}) \pm [\mathbb{E}^2(\mathbf{Q}) - \mathbb{F}^2(\mathbf{Q})]^{1/2}\}$

Case	Requirements for $\hat{\mathbf{p}}_x \perp \hat{\mathbf{n}}$	Equations
3	None	$|N(|\mathbf{Q}|, 0°)|^2 = \mathbb{A}(|\mathbf{Q}|, 0°)$
		$|N(|\mathbf{Q}|, 90°)|^2 + |M_{x,\hat{\mathbf{p}}_x\perp\hat{\mathbf{n}}}(|\mathbf{Q}|, 90°)|^2 = \mathbb{A}(|\mathbf{Q}|, 90°)$
		$|M_{y,\hat{\mathbf{p}}_x\perp\hat{\mathbf{n}}}(|\mathbf{Q}|, 0°)|^2 + |M_{z,\hat{\mathbf{p}}_x\perp\hat{\mathbf{n}}}(|\mathbf{Q}|, 0°)|^2 = \mathbb{C}(|\mathbf{Q}|, 0°)$
		$|M_{z,\hat{\mathbf{p}}_x\perp\hat{\mathbf{n}}}(|\mathbf{Q}|, 90°)|^2 = \mathbb{C}(|\mathbf{Q}|, 90°)$
		$|N(\mathbf{Q})|^2 - \tan^2(\theta)|M_{z,\hat{\mathbf{p}}_x\perp\hat{\mathbf{n}}}(\mathbf{Q})|^2 = \mathbb{A}(\mathbf{Q}) - \tan^2(\theta)\,\mathbb{C}(\mathbf{Q})$
4	Isotropic $|N(\mathbf{Q})|$	$|N(\mathbf{Q})|^2 = |N(|\mathbf{Q}|, 0°)|^2 = \mathbb{A}(|\mathbf{Q}|, 0°)$
		$|M_{x,\hat{\mathbf{p}}_x\perp\hat{\mathbf{n}}}(|\mathbf{Q}|, 90°)|^2 = \mathbb{A}(|\mathbf{Q}|, 90°) - \mathbb{A}(|\mathbf{Q}|, 0°)$
5A	Isotropic $|N(\mathbf{Q})|$	$|N(\mathbf{Q})|^2 = |N(|\mathbf{Q}|, 0°)|^2 = \mathbb{A}(|\mathbf{Q}|, 0°)$
	$|\overline{\cos}(\varphi_N - \varphi_{M_x,\hat{\mathbf{p}}_x\perp\hat{\mathbf{n}}})| \Rightarrow 1$	$|M_{x,\hat{\mathbf{p}}_x\perp\hat{\mathbf{n}}}(\mathbf{Q})|^2 = \mathbb{B}^2(\mathbf{Q})/4\sin^4(\theta)\,\mathbb{A}(|\mathbf{Q}|, 0°)$
	$|N(\mathbf{Q})|\,|M_{y,\hat{\mathbf{p}}_x\perp\hat{\mathbf{n}}}(\mathbf{Q})|\,\overline{\cos}(\varphi_N - \varphi_{M_y,\hat{\mathbf{p}}_x\perp\hat{\mathbf{n}}}) \Rightarrow 0$	$\cos^4(\theta)|M_{y,\hat{\mathbf{p}}_x\perp\hat{\mathbf{n}}}(\mathbf{Q})|^2 + |M_{z,\hat{\mathbf{p}}_x\perp\hat{\mathbf{n}}}(\mathbf{Q})|^2 = \mathbb{C}(\mathbf{Q}) - |M_{x,\hat{\mathbf{p}}_x\perp\hat{\mathbf{n}}}(\mathbf{Q})|^2\sin^2(\theta)\cos^4(\theta)$
5B	Isotropic $|N(\mathbf{Q})|$	$|N(\mathbf{Q})|^2 = |N(|\mathbf{Q}|, 0°)|^2 = \mathbb{A}(|\mathbf{Q}|, 0°)$
	$|\overline{\cos}(\varphi_N - \varphi_{M_x,\hat{\mathbf{p}}_x\perp\hat{\mathbf{n}}})| \Rightarrow 1$	$|M_{x,\hat{\mathbf{p}}_x\perp\hat{\mathbf{n}}}(\mathbf{Q})|^2 = \mathbb{B}'^2(\mathbf{Q})/4\sin^4(\theta)\,\mathbb{A}(|\mathbf{Q}|, 0°)$
	Net (or zero) M_y	
6A	$|M_{x,\hat{\mathbf{p}}_x\perp\hat{\mathbf{n}}}(\mathbf{Q})|^2 = |M_{y,\hat{\mathbf{p}}_x\perp\hat{\mathbf{n}}}(\mathbf{Q})|^2 = |M_{z,\hat{\mathbf{p}}_x\perp\hat{\mathbf{n}}}(\mathbf{Q})|^2 \equiv |M_{\text{equiv}}(\mathbf{Q})|^2$	$|M_{\text{equiv}}|^2 = \mathbb{C}(\mathbf{Q})/[1 + \cos^2(\theta) - 2\sin(\theta)\cos^3(\theta)]$
	$|M_{x,\hat{\mathbf{p}}_x\perp\hat{\mathbf{n}}}|\,|M_{y,\hat{\mathbf{p}}_x\perp\hat{\mathbf{n}}}|\,\overline{\cos}(\varphi_{M_x,\hat{\mathbf{p}}_x\perp\hat{\mathbf{n}}} - \varphi_{M_y,\hat{\mathbf{p}}_x\perp\hat{\mathbf{n}}}) \Rightarrow 0$	$|N(\mathbf{Q})|^2 = \mathbb{A}(\mathbf{Q}) - \sin^2(\theta)|M_{\text{equiv}}|^2$
6B	$|M_{x,\hat{\mathbf{p}}_x\perp\hat{\mathbf{n}}}|^2 = |M_{y,\hat{\mathbf{p}}_x\perp\hat{\mathbf{n}}}|^2 = |M_{z,\hat{\mathbf{p}}_x\perp\hat{\mathbf{n}}}|^2 \equiv |M_{\text{equiv}}|^2$	$|M_{\text{equiv}}(\mathbf{Q})|^2 = \mathbb{C}(\mathbf{Q})/[1 + \cos^2(\theta)]$
	$\overline{\cos}(\varphi_{M_x} - \varphi_{M_y}) \Rightarrow 1$	$|N(\mathbf{Q})|^2 = \mathbb{A}(\mathbf{Q}) - |M_{\text{equiv}}|^2[\sin^2(\theta) - 2\sin^3(\theta)\cos(\theta)]$
7	$|M_{y,\hat{\mathbf{p}}_x\perp\hat{\mathbf{n}}}(\mathbf{Q})|$ and $|M_{z,\hat{\mathbf{p}}_x\perp\hat{\mathbf{n}}}(\mathbf{Q})| \Rightarrow 0$	$|M_{x,\hat{\mathbf{p}}_x\perp\hat{\mathbf{n}}}(\mathbf{Q})|^2 = \mathbb{C}(\mathbf{Q})/\sin^2(\theta)\cos^2(\theta)$
		$|N(\mathbf{Q})|^2 = \mathbb{A}(\mathbf{Q}) - |M_{x,\hat{\mathbf{p}}_x\perp\hat{\mathbf{n}}}(\mathbf{Q})|^2\sin^4(\theta)$
8A	$|\overline{\cos}(\varphi_N - \varphi_{M_x,\hat{\mathbf{p}}_x\perp\hat{\mathbf{n}}})| \Rightarrow 1$	$|N(\mathbf{Q})|^2 = \frac{1}{2}\{\mathbb{A}(\mathbf{Q}) \pm [\mathbb{A}^2(\mathbf{Q}) - \mathbb{B}^2(\mathbf{Q})]^{1/2}\}$
	$|N(\mathbf{Q})|\,|M_{y,\hat{\mathbf{p}}_x\perp\hat{\mathbf{n}}}(\mathbf{Q})|\,\overline{\cos}(\varphi_N - \varphi_{M_y,\hat{\mathbf{p}}_x\perp\hat{\mathbf{n}}}) \Rightarrow 0$	$|M_{x,\hat{\mathbf{p}}_x\perp\hat{\mathbf{n}}}(\mathbf{Q})|^2 = \mathbb{B}^2(\mathbf{Q})/4\sin^4(\theta)\,|N(\mathbf{Q})|^2$
8B	$|\overline{\cos}(\varphi_N - \varphi_{M_x,\hat{\mathbf{p}}_x\perp\hat{\mathbf{n}}})| \Rightarrow 1$	$|N(\mathbf{Q})|^2 = \frac{1}{2}\{\mathbb{A}(\mathbf{Q}) \pm [\mathbb{A}^2(\mathbf{Q}) - \mathbb{B}^2(\mathbf{Q})]^{1/2}\}$
	Net (or zero) $M_{y,\hat{\mathbf{p}}_x\perp\hat{\mathbf{n}}}(\mathbf{Q})$	$|M_{x,\hat{\mathbf{p}}_x\perp\hat{\mathbf{n}}}(\mathbf{Q})|^2 = \mathbb{B}'^2(\mathbf{Q})/4\sin^4(\theta)\,|N(\mathbf{Q})|^2$
9A	$|\overline{\cos}(\varphi_N - \varphi_{M_y,\hat{\mathbf{p}}_x\perp\hat{\mathbf{n}}})| \Rightarrow 1$	$|N(\mathbf{Q})|^2 = \frac{1}{2}\{\mathbb{A}(\mathbf{Q}) \pm [\mathbb{A}^2(\mathbf{Q}) - \mathbb{B}^2(\mathbf{Q})]^{1/2}\}$
	$|N(\mathbf{Q})|\,|M_{x,\hat{\mathbf{p}}_x\perp\hat{\mathbf{n}}}(\mathbf{Q})|\,\overline{\cos}(\varphi_N - \varphi_{M_x,\hat{\mathbf{p}}_x\perp\hat{\mathbf{n}}}) \Rightarrow 0$	$|M_{y,\hat{\mathbf{p}}_x\perp\hat{\mathbf{n}}}(\mathbf{Q})|^2 = \mathbb{B}^2(\mathbf{Q})/4\sin^2(\theta)\cos^2(\theta)\,|N(\mathbf{Q})|^2$
9B	$|\overline{\cos}(\varphi_N - \varphi_{M_y,\hat{\mathbf{p}}_x\perp\hat{\mathbf{n}}})| \Rightarrow 1$	$|N(\mathbf{Q})|^2 = \frac{1}{2}\{\mathbb{A}(\mathbf{Q}) \pm [\mathbb{A}^2(\mathbf{Q}) - \mathbb{B}^2(\mathbf{Q})]^{1/2}\}$
	Net (or zero) $|M_{x,\hat{\mathbf{p}}_x\perp\hat{\mathbf{n}}}(\mathbf{Q})|$	$|M_{y,\hat{\mathbf{p}}_x\perp\hat{\mathbf{n}}}(\mathbf{Q})|^2 = \mathbb{B}''^2(\mathbf{Q})/4\sin^2(\theta)\cos^2(\theta)\,|N(\mathbf{Q})|^2$
10A	$|\overline{\cos}(\varphi_N - \varphi_{M_x,\hat{\mathbf{p}}_x\perp\hat{\mathbf{n}}})| \Rightarrow 1$	$|N(\mathbf{Q})|^2, \beta(\mathbf{Q}) = \frac{1}{2}\{\mathbb{A}(\mathbf{Q}) \pm [\mathbb{A}^2(\mathbf{Q}) - \mathbb{B}^2(\mathbf{Q})]^{1/2}\}$ with
	$|\overline{\cos}(\varphi_N - \varphi_{M_y,\hat{\mathbf{p}}_x\perp\hat{\mathbf{n}}})| \Rightarrow 1$	$|M_{z,\hat{\mathbf{p}}_x\perp\hat{\mathbf{n}}}(\mathbf{Q})|^2 = \mathbb{C}(\mathbf{Q}) - \beta(\mathbf{Q})/\tan^2(\theta)$
10B	Net or zero $M_{x,\hat{\mathbf{p}}_x\perp\hat{\mathbf{n}}}(\mathbf{Q})$	$|N(\mathbf{Q})|^2, \beta(\mathbf{Q}) = \frac{1}{2}\{\mathbb{A}(\mathbf{Q}) \pm [\mathbb{A}^2(\mathbf{Q}) - \mathbb{B}^2(\mathbf{Q})]^{1/2}\}$
	Net or zero $M_{y,\hat{\mathbf{p}}_x\perp\hat{\mathbf{n}}}(\mathbf{Q})$	$|M_{z,\hat{\mathbf{p}}_x\perp\hat{\mathbf{n}}}(\mathbf{Q})|^2 = \mathbb{C}'(\mathbf{Q}) - \beta(\mathbf{Q})/\tan^2(\theta)$
	$|\overline{\cos}(\varphi_N - \varphi_{M_x,\hat{\mathbf{p}}_x\perp\hat{\mathbf{n}}})| \Rightarrow 1$	$|M_{x,\hat{\mathbf{p}}_x\perp\hat{\mathbf{n}}}(\mathbf{Q})|^2 = \mathbb{B}'^2(\mathbf{Q})/4\sin^4(\theta)\,|N(\mathbf{Q})|^2$
	$|\overline{\cos}(\varphi_N - \varphi_{M_y,\hat{\mathbf{p}}_x\perp\hat{\mathbf{n}}})| \Rightarrow 1$	$|M_{y,\hat{\mathbf{p}}_x\perp\hat{\mathbf{n}}}(\mathbf{Q})|^2 = \mathbb{B}''^2(\mathbf{Q})/4\sin^2(\theta)\cos^2(\theta)\,|N(\mathbf{Q})|^2$

$|M_{z,\hat{\mathbf{p}}_z\|\hat{\mathbf{n}}}(\mathbf{Q})|^2$ at lower field conditions. Note, however, that this approach extracts the Fourier transform of the net moments pointing along $\mathbf{Z}$, rather than the Fourier transform of the magnetic domains that point along $\pm\mathbf{Z}$ that direct measurement of $|M_Z|^2$ would yield. These extractions may vary considerably when the sample is far from magnetic saturation.

6.3. Case 3: general $\hat{\mathbf{p}} \perp \hat{\mathbf{n}}$

Since $\hat{\mathbf{p}} \parallel \hat{\mathbf{n}}$ does not always allow for unique separation of the magnetic components, we shall focus the remainder of the paper on the $\hat{\mathbf{p}} \perp \hat{\mathbf{n}}$ geometry. The angular-dependent scattering equations of Table 1 simplify greatly along the coordinate axes, defined by $\hat{\mathbf{p}}$ and $\hat{\mathbf{n}}$, in this most general case (Case 3, Table 4) as

$$|N(|\mathbf{Q}|, 0°)|^2 = \mathbb{A}(|\mathbf{Q}|, 0°),$$
$$|N(|\mathbf{Q}|, 90°)|^2 + |M_{x,\hat{\mathbf{p}}_x \perp \hat{\mathbf{n}}}(|\mathbf{Q}|, 90°)|^2 = \mathbb{A}(|\mathbf{Q}|, 90°),$$
$$|M_{y,\hat{\mathbf{p}}_x \perp \hat{\mathbf{n}}}(|\mathbf{Q}|, 0°)|^2 + |M_{z,\hat{\mathbf{p}}_x \perp \hat{\mathbf{n}}}(|\mathbf{Q}|, 0°)|^2 = \mathbb{C}(|\mathbf{Q}|, 0°),$$
$$|M_{z,\hat{\mathbf{p}}_x \perp \hat{\mathbf{n}}}(|\mathbf{Q}|, 90°)|^2 = \mathbb{C}(|\mathbf{Q}|, 90°). \quad (14)$$

A 2:1 symmetry would be expected for the spin-flip scattering along $\theta = 0°$ and $\theta = 90°$, respectively, if $|M_{z,\hat{\mathbf{p}}_z \perp \hat{\mathbf{n}}}(\mathbf{Q})|^2$ is isotropic and $|M_{z,\hat{\mathbf{p}}_z \perp \hat{\mathbf{n}}}(\mathbf{Q})|^2 = |M_{y,\hat{\mathbf{p}}_x \perp \hat{\mathbf{n}}}(\mathbf{Q})|^2$. Additionally, a partial separation of terms for arbitrary θ involving only $|N(\mathbf{Q})|^2$ and $|M_{z,\hat{\mathbf{p}}_x \perp \hat{\mathbf{n}}}(\mathbf{Q})|^2$ (Case 3, Table 4) can be performed using

$$|N(\mathbf{Q})|^2 - \tan^2(\theta)\,|M_{z,\hat{\mathbf{p}}_x \perp \hat{\mathbf{n}}}(\mathbf{Q})|^2 = \mathbb{A}(\mathbf{Q}) - \tan^2(\theta)\,\mathbb{C}(\mathbf{Q}) \quad (15)$$

for $\theta \neq 90, 270°$. Equation (15) could be particularly useful for determining whether $|N(\mathbf{Q})|^2$ is isotropic if $|N(\mathbf{Q})| \gg |M_{z,\hat{\mathbf{p}}_x \perp \hat{\mathbf{n}}}(\mathbf{Q})|$ or if $|M_{z,\hat{\mathbf{p}}_x \perp \hat{\mathbf{n}}}(\mathbf{Q})|$ is constant as a function of θ. For samples that do not deform when the direction of the applied field is altered, equations (14) and (15) in conjunction with rotation of the sample (or equivalently rotation of the applied field from $\mathbf{X}$ to $\mathbf{Y}$) would allow $|N(|\mathbf{Q}|, 0°)|^2$, $|N(|\mathbf{Q}|, 90°)|^2$ and $|M_{x,\hat{\mathbf{p}}_x \perp \hat{\mathbf{n}}}(|\mathbf{Q}|, 90°)|^2$, $|M_{x,\hat{\mathbf{p}}_x \perp \hat{\mathbf{n}}}(|\mathbf{Q}|, 0°)|^2$ to be resolved at any field condition, as well as $|M_{z,\hat{\mathbf{p}}_x \perp \hat{\mathbf{n}}}(|\mathbf{Q}|, 0°)|^2$ to be separated from $|M_{y,\hat{\mathbf{p}}_x \perp \hat{\mathbf{n}}}(|\mathbf{Q}|, 0°)|^2$.

7. Structurally isotropic samples

Structurally isotropic samples are often the most common and simplest. Structural isotropy in this context means that the structural morphology and resulting scattering at any particular $|\mathbf{Q}|$ is invariant as a function of angle, θ (e.g. the scattering from a spherically symmetric object). This condition can be checked by rotating the sample and determining whether $|N(|\mathbf{Q}|, 0°)|^2 = \mathbb{A}(|\mathbf{Q}|, 0°)$ remains constant. Similarly, magnetic isotropy implies that the magnetic structures composed of the projections of moments aligned along axes x, y or z each retain a constant spatial distribution when viewed in any particular $\mathbf{Q}$ direction. This is most likely to be achieved in systems showing negligible remanence and at very small applied magnetic guide fields, though it is difficult to check for magnetic anisotropy by means of simple sample rotation about $\hat{\mathbf{p}}$ because it involves changing the projection of the applied magnetic field direction onto the sample, which in turn may affect the underlying magnetic response. Structural isotropy does not necessarily imply magnetic isotropy.

7.1. Case 4: isotropic N for $\hat{\mathbf{p}} \perp \hat{\mathbf{n}}$

If it is known from *a priori* knowledge or experimental PASANS evidence that structural and magnetic isotropy exist, then one can use the angular symmetries presented in Table 2 to simultaneously identify and fit the θ dependence of each contributing scattering term (Wiedenmann, 2005; Michels & Weissmüller, 2008; Dufour *et al.*, 2011), with the caveat that the sign of interference contributions containing odd numbers of $\sin(\theta)$ and $\cos(\theta)$ terms may change sign with quadrant as discussed previously (refer to Table 2). Alternatively, it may be preferable to separate each term unambiguously. With

knowledge that the sample is structurally isotropic [*i.e.* $|N(|\mathbf{Q}|, 0°)|^2 = |N(|\mathbf{Q}|, 90°)|^2$], the $|M_{x,\hat{\mathbf{p}}_x \perp \hat{\mathbf{n}}}(|\mathbf{Q}|, 90°)|^2$ and $|N(|\mathbf{Q}|, \theta)|^2$ terms may be separated (Case 4, Table 4) using

$$|M_{x,\hat{\mathbf{p}}_x \perp \hat{\mathbf{n}}}(|\mathbf{Q}|, 90°)|^2 = \mathbb{A}(|\mathbf{Q}|, 90°) - \mathbb{A}(|\mathbf{Q}|, 0°),$$
$$|N(\mathbf{Q})|^2 = |N(|\mathbf{Q}|, 0°)|^2. \quad (16)$$

This is the first of many unambiguous separations of magnetic and structural scattering that polarization analysis affords, and it can be quite important in determining magnetic behavior, especially since the structural scattering typically dominates the magnetic scattering.

7.2. Cases 5A–5B: isotropic N in phase with M_X for $\hat{\mathbf{p}} \perp \hat{\mathbf{n}}$

In addition to structural isotropy, if it were known that $N(\mathbf{Q})$ and $M_{x,\hat{\mathbf{p}}_x \perp \hat{\mathbf{n}}}(\mathbf{Q})$ were in phase [*i.e.* $|\overline{\cos}(\varphi_N - \varphi_{M_{x,\hat{\mathbf{p}}_x \perp \hat{\mathbf{n}}}})| \Rightarrow 1$, where the nuclear and magnetic morphologies share the same structure factors, as is expected under conditions of magnetic saturation] and also that $N(\mathbf{Q})$ and $M_{y,\hat{\mathbf{p}}_x \perp \hat{\mathbf{n}}}(\mathbf{Q})$ were out of phase [*i.e.* $|\overline{\cos}(\varphi_N - \varphi_{M_{y,\hat{\mathbf{p}}_x \perp \hat{\mathbf{n}}}})| \Rightarrow 0$, as expected for randomly oriented $M_{y,\hat{\mathbf{p}}_x \perp \hat{\mathbf{n}}}(\mathbf{Q})$ domains pointing along $+\mathbf{Y}$ and $-\mathbf{Y}$ with equal probability] or that $M_{y,\hat{\mathbf{p}}_x \perp \hat{\mathbf{n}}}(\mathbf{Q}) \Rightarrow 0$, then (case 5A)

$$|M_{x,\hat{\mathbf{p}}_x \perp \hat{\mathbf{n}}}(\mathbf{Q})|^2 = \frac{\mathbb{B}^2(\mathbf{Q})}{4\sin^2(\theta)\,\mathbb{A}(|\mathbf{Q}|, 0°)} \quad (17)$$

for all $\theta \neq 0, 180°$. As a partial check, if $|M_{x,\hat{\mathbf{p}}_x \perp \hat{\mathbf{n}}}(\mathbf{Q})| > 0$ and it is in phase with $|N(\mathbf{Q})|^2$, then $\mathbb{B}(|\mathbf{Q}|, 90°)$ (Table 1) should also be > 0. Similarly, if $|M_{y,\hat{\mathbf{p}}_x \perp \hat{\mathbf{n}}}(\mathbf{Q})| = 0$ or is out of phase with $|N(\mathbf{Q})|^2$, then $\mathbb{B}(|\mathbf{Q}|, 0°)$ (Table 1) should be equal to 0.

The mere observation of $|\mathbb{B}(\mathbf{Q})| > 0$ implies some level of net magnetism along the X or Y axis and matched phase between the structure and magnetism, and it provides an indirect measure of the degree of magnetic saturation as $\theta \Rightarrow 90°$. However, it is difficult to quantify conclusively from $\mathbb{B}(\mathbf{Q})$ alone the net magnetic moment since a partial dephasing between $M_{x,\hat{\mathbf{p}}_x \perp \hat{\mathbf{n}}}(\mathbf{Q})$ and $N(\mathbf{Q})$, for example, would mimic a reduction in $|M_{x,\hat{\mathbf{p}}_x \perp \hat{\mathbf{n}}}(\mathbf{Q})|$. As a result of this possible ambiguity, it is a good idea to check the magnitude of $|M_{x,\hat{\mathbf{p}}_x \perp \hat{\mathbf{n}}}(|\mathbf{Q}|, 90°)|^2$ obtained from equation (17) with equation (16), which is not dependent upon achieving any level of phase matching (though it is more sensitive to any subtle instrumental non-uniformity across the detector). Additionally, it shall be shown that $M_{x,\hat{\mathbf{p}}_x \perp \hat{\mathbf{n}}}(\mathbf{Q})$ determined from equation (17) is often more statistically significant than that determined from equation (16) for situations where $|N(\mathbf{Q})| \gg |M_{x,\hat{\mathbf{p}}_x \perp \hat{\mathbf{n}}}(\mathbf{Q})|$.

If the above phase conditions are met, this also implies that $M_{x,\hat{\mathbf{p}}_x \perp \hat{\mathbf{n}}}(\mathbf{Q})$ is out of phase with $M_{y,\hat{\mathbf{p}}_x \perp \hat{\mathbf{n}}}(\mathbf{Q})$ (or the latter is zero). Under these circumstances we can obtain information about the perpendicular magnetism at all θ (Case 5A) using

$$\cos^4(\theta)M_{y,\hat{\mathbf{p}}_x \perp \hat{\mathbf{n}}}(\mathbf{Q}) + M_{z,\hat{\mathbf{p}}_x \perp \hat{\mathbf{n}}}(\mathbf{Q}) = \mathbb{C}(\mathbf{Q}) - |M_{x,\hat{\mathbf{p}}_x \perp \hat{\mathbf{n}}}(\mathbf{Q})|^2$$
$$\times \sin^2(\theta)\cos^4(\theta). \quad (18)$$

It is likely that $M_{y,\hat{\mathbf{p}}_x \perp \hat{\mathbf{n}}}(\mathbf{Q})$ and $M_{z,\hat{\mathbf{p}}_x \perp \hat{\mathbf{n}}}(\mathbf{Q})$ are equivalent. An observation of a 2:1 dependence for $\mathbb{C}'(|\mathbf{Q}|, 0°)$ to $\mathbb{C}'(|\mathbf{Q}|, 90°)$

would be a good indicator of similarity, though lack of this 2:1 dependence does not preclude $M_{y,\hat{\mathbf{p}}_x \perp \hat{\mathbf{n}}}(\mathbf{Q}) = M_{z,\hat{\mathbf{p}}_x \perp \hat{\mathbf{n}}}(\mathbf{Q})$ as θ variation within the magnetic morphology may be involved.

If the phase between $M_{y,\hat{\mathbf{p}}_x \perp \hat{\mathbf{n}}}(\mathbf{Q})$ and $N(\mathbf{Q})$ is unknown, yet it is known that $M_{y,\hat{\mathbf{p}}_x \perp \hat{\mathbf{n}}}(\mathbf{Q})$ has a net moment, then any nonzero $N(\mathbf{Q})$–$M_{y,\hat{\mathbf{p}}_x \perp \hat{\mathbf{n}}}(\mathbf{Q})$ interference term will appear in $\mathbb{B}''(\mathbf{Q})$ and not in $\mathbb{B}'(\mathbf{Q})$ (Table 3). Under this condition $|M_{y,\hat{\mathbf{p}}_x \perp \hat{\mathbf{n}}}(\mathbf{Q})|^2$ is solvable (Case 5B) using

$$|M_{x,\hat{\mathbf{p}}_x \perp \hat{\mathbf{n}}}(\mathbf{Q})|^2 = \frac{\mathbb{B}'^2(\mathbf{Q})}{4\sin^2(\theta)\,\mathbb{A}(|\mathbf{Q}|, 0°)}. \tag{19}$$

8. Structure and magnetic phase demonstration

To elucidate the importance of the phase and interference, consider the PASANS example consisting of randomly
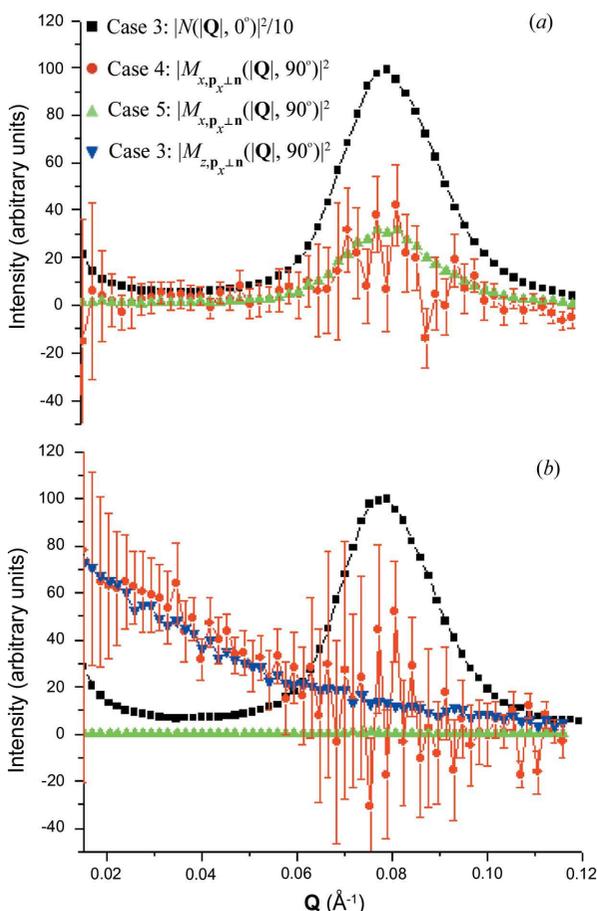

Figure 3
Nuclear and magnetic separation for close-packed 9 nm Fe_3O_4 nanoparticles. (a) Under conditions of saturation, Cases 4 or 5A from Table 4 can be used to extract $|M_{x,\hat{\mathbf{p}}_x \perp \hat{\mathbf{n}}}(|\mathbf{Q}|, 90°)|^2$. (b) At remanence, $|M_{x,\hat{\mathbf{p}}_x \perp \hat{\mathbf{n}}}(|\mathbf{Q}|, 90°)|^2 = |M_{z,\hat{\mathbf{p}}_x \perp \hat{\mathbf{n}}}(|\mathbf{Q}|, 90°)|^2$, with the latter determined using Case 3. However, Case 5A (unlike Case 4) fails to correctly produce $|M_{x,\hat{\mathbf{p}}_x \perp \hat{\mathbf{n}}}(|\mathbf{Q}|, 90°)|^2$ because the equal and oppositely oriented magnetic domains cause $\overline{\cos}(\varphi_N - \varphi_{M_x}) \Rightarrow 0$. For (a) and (b), subtraction of a large $|N(\mathbf{Q})|^2$ peak causes Case 4 to be statistically noisier than other methods for determining the magnetic morphology, as indicated by the errors bars representing one standard deviation.

oriented, structurally isotropic, close-packed crystallites composed of 9 nm Fe_3O_4 nanospheres (Krycka *et al.*, 2010) which at magnetic saturation produced $(\rho_M/\rho_N)^2 < 0.04$. (The sample choice is fairly unimportant, but the system selected provides a good demonstration.) In an applied saturating field of 1.25 T, equations (16) and (17) both return $|M_{x,\hat{\mathbf{p}}_x \perp \hat{\mathbf{n}}}(\mathbf{Q})|^2$ (Fig. 2a) of roughly equivalent shape and magnitude. However, the interference term of $|N(\mathbf{Q})|\,|M_{x,\hat{\mathbf{p}}_x \perp \hat{\mathbf{n}}}(\mathbf{Q})|$ is much stronger than $|M_{x,\hat{\mathbf{p}}_x \perp \hat{\mathbf{n}}}(\mathbf{Q})|^2$ alone, and the result is that the use of equation (17) produces a more statistically significant measurement than equation (16) for the same data (Fig. 3a).

In contrast, let us examine scattering from the same sample, but at a remanent field of 0.005 T. Now equation (16) returns a nonzero $|M_{x,\hat{\mathbf{p}}_x \perp \hat{\mathbf{n}}}(\mathbf{Q})|^2$ arising from long-range domains, while equation (17) suggests that $|M_{x,\hat{\mathbf{p}}_x \perp \hat{\mathbf{n}}}(\mathbf{Q})|^2$ is negligible (Fig. 3b). The former, however, agrees with the spin-flip measured value $|M_{z,\hat{\mathbf{p}}_x \perp \hat{\mathbf{n}}}|^2$ [equation (14)] that would be expected for a structurally isotropic sample near zero field. The reason that equation (17) failed to isolate $|M_{x,\hat{\mathbf{p}}_x \perp \hat{\mathbf{n}}}(\mathbf{Q})|^2$ correctly is that the magnetic scattering centers have formed domains that are randomly oriented throughout the sample. The sign of $\overline{\cos}(\varphi_N - \varphi_{M_x,\hat{\mathbf{p}}_x \perp \hat{\mathbf{n}}})$ is, thus, randomly distributed from +1 to −1, and a sum of all the domains cancels to zero. Simply put, equation (17) measures the net $M_{x,\hat{\mathbf{p}}_x \perp \hat{\mathbf{n}}}(\mathbf{Q})$ magnetization, while equation (16) reveals $M_{x,\hat{\mathbf{p}}_x \perp \hat{\mathbf{n}}}(\mathbf{Q})$ magnetic domains that are both parallel and antiparallel to the guide field. Thus, understanding how these interference terms behave when interpreting the scattering patterns is of paramount importance to correctly interpreting PASANS data.

9. Structurally anisotropic samples

While analysis involving $\theta = 0°$ and $\theta = 90°$ comparisons may adequately cover a variety of isotropic systems, such an imposition excludes important classes of samples that are anisotropic by design. Most notable among these systems are solvated particles under the influence of an applied magnetic field or flow gradient, patterned media that are not spherically symmetric within the XY plane, magnetostrictive systems, and crystalline materials with long-range order. By knowing something about the sample's response to applied field, however, one can build from Case 3, Table 4 so as to include scattering information at angles away from the coordinate axes.

9.1. Cases 6A–6B: $M_X(\mathbf{Q}) = M_Y(\mathbf{Q}) = M_Z(\mathbf{Q})$ for $\hat{\mathbf{p}} \perp \hat{\mathbf{n}}$

If it is known that the magnetic moments are randomly distributed (typical of systems without a remanent moment in zero or near-zero applied fields), then the average magnetic distribution along any given direction, $|M_{x,\hat{\mathbf{p}}_x \perp \hat{\mathbf{n}}}(\mathbf{Q})| = |M_{y,\hat{\mathbf{p}}_x \perp \hat{\mathbf{n}}}(\mathbf{Q})| = |M_{z,\hat{\mathbf{p}}_x \perp \hat{\mathbf{n}}}(\mathbf{Q})| \equiv |M_{\mathrm{equiv}}(\mathbf{Q})|$, is separable from $N(\mathbf{Q})$ using $\mathbb{A}$ and $\mathbb{C}$ (Table 1) along with knowledge of the relative phase between $M_{x,\hat{\mathbf{p}}_x \perp \hat{\mathbf{n}}}(\mathbf{Q})$ and $M_{y,\hat{\mathbf{p}}_x \perp \hat{\mathbf{n}}}(\mathbf{Q})$. If $M_{x,\hat{\mathbf{p}}_x \perp \hat{\mathbf{n}}}(\mathbf{Q})$ and $M_{y,\hat{\mathbf{p}}_x \perp \hat{\mathbf{n}}}(\mathbf{Q})$ are out of phase, as for a series of randomly distributed domains (Case 6A), then

$$|M_{\text{equiv}}|^2 = \mathbb{C}(\mathbf{Q})/[1 + \cos^2(\theta) - 2\sin(\theta)\cos^3(\theta)],$$
$$|N(\mathbf{Q})|^2 = \mathbb{A}(\mathbf{Q}) - \sin^2(\theta)|M_{\text{equiv}}|^2. \tag{20}$$

Instead, if $M_{x,\hat{\mathbf{p}}_x \perp \hat{\mathbf{n}}}(\mathbf{Q})$ and $M_{y,\hat{\mathbf{p}}_x \perp \hat{\mathbf{n}}}(\mathbf{Q})$ are in phase, as for magnetic domains or nanoparticles each containing $M_{x,\hat{\mathbf{p}}_x \perp \hat{\mathbf{n}}}(\mathbf{Q})$ and $M_{y,\hat{\mathbf{p}}_x \perp \hat{\mathbf{n}}}(\mathbf{Q})$ structures that are the same from domain to domain or particle to particle (Case 6B), then

$$|M_{\text{equiv}}|^2 = \mathbb{C}(\mathbf{Q})/[1 + \cos^2(\theta)],$$
$$|N(\mathbf{Q})|^2 = \mathbb{A}(\mathbf{Q}) - |M_{\text{equiv}}|^2[\sin^2(\theta) - 2\sin^3(\theta)\cos(\theta)]. \tag{21}$$

Other related conditions should lie somewhere between the extremes of Cases 6A and 6B. Unfortunately, it may be difficult to determine the degree to which $M_{x,\hat{\mathbf{p}}_x \perp \hat{\mathbf{n}}}(\mathbf{Q})$ and $M_{y,\hat{\mathbf{p}}_x \perp \hat{\mathbf{n}}}(\mathbf{Q})$ are correlated since the term found in $\mathbb{C}(\mathbf{Q})$ is combined with other magnetic terms that may vary as a function of θ. However, $\mathbb{C}''(\mathbf{Q})$ (Table 3) can provide an indication of phase relations as long as $M_{x,\hat{\mathbf{p}}_x \perp \hat{\mathbf{n}}}(\mathbf{Q})$ and $M_{y,\hat{\mathbf{p}}_x \perp \hat{\mathbf{n}}}(\mathbf{Q})$ each contain net moments.

9.2. Case 7: minimal perpendicular magnetism for $\hat{\mathbf{p}} \perp \hat{\mathbf{n}}$

If $M_{y,\hat{\mathbf{p}}_x \perp \hat{\mathbf{n}}}(\mathbf{Q})$ and $M_{z,\hat{\mathbf{p}}_x \perp \hat{\mathbf{n}}}(\mathbf{Q})$ are negligible (e.g. if they are composed of small, equal and oppositely oriented domains without a periodic modulation), then $|M_{x,\hat{\mathbf{p}}_x \perp \hat{\mathbf{n}}}(\mathbf{Q})|^2$ may be isolated in the spin-flip scattering, $\mathbb{C}$, while $|N(\mathbf{Q})|^2$ can be obtained from the subtraction of $|M_{x,\hat{\mathbf{p}}_x \perp \hat{\mathbf{n}}}(\mathbf{Q})|^2$ from the non-spin-flip scattering, $\mathbb{A}$ (Table 1), using (Case 7)

$$|M_{x,\hat{\mathbf{p}}_x \perp \hat{\mathbf{n}}}(\mathbf{Q})|^2 = \mathbb{C}(\mathbf{Q})/\sin^2(\theta)\cos^2(\theta),$$
$$|N(\mathbf{Q})|^2 = \mathbb{A}(\mathbf{Q}) - |M_{x,\hat{\mathbf{p}}_x \perp \hat{\mathbf{n}}}(\mathbf{Q})|^2 \sin^4(\theta). \tag{22}$$

As always, $|M_{x,\hat{\mathbf{p}}_x \perp \hat{\mathbf{n}}}(\mathbf{Q})|^2$ cannot be measured directly along $\theta = 0°$ since only moments perpendicular to $\mathbf{Q}$ are measurable (Halpern–Johnson vector selection rules).

9.3. Cases 8A–8B: N and M_X in phase for $\hat{\mathbf{p}} \perp \hat{\mathbf{n}}$

If $M_{x,\hat{\mathbf{p}}_x \perp \hat{\mathbf{n}}}(\mathbf{Q})$ is sufficiently long ranged so as to be in phase with $N(\mathbf{Q})$ (as would be expected near saturation), but $M_{y,\hat{\mathbf{p}}_x \perp \hat{\mathbf{n}}}(\mathbf{Q}) \Rightarrow 0$ or it is out of phase with $N(\mathbf{Q})$, then $M_{x,\hat{\mathbf{p}}_x \perp \hat{\mathbf{n}}}(\mathbf{Q})$ and $N(\mathbf{Q})$ may be solved using quadratic equations of $\mathbb{A}$ and $\mathbb{B}$ (Table 1) using (Case 8A)

- ■ $|N(\mathbf{Q})|^2/70$
- ● $|M_{x,\hat{\mathbf{p}}_x \perp \hat{\mathbf{n}}}(\mathbf{Q})|^2/2.5$
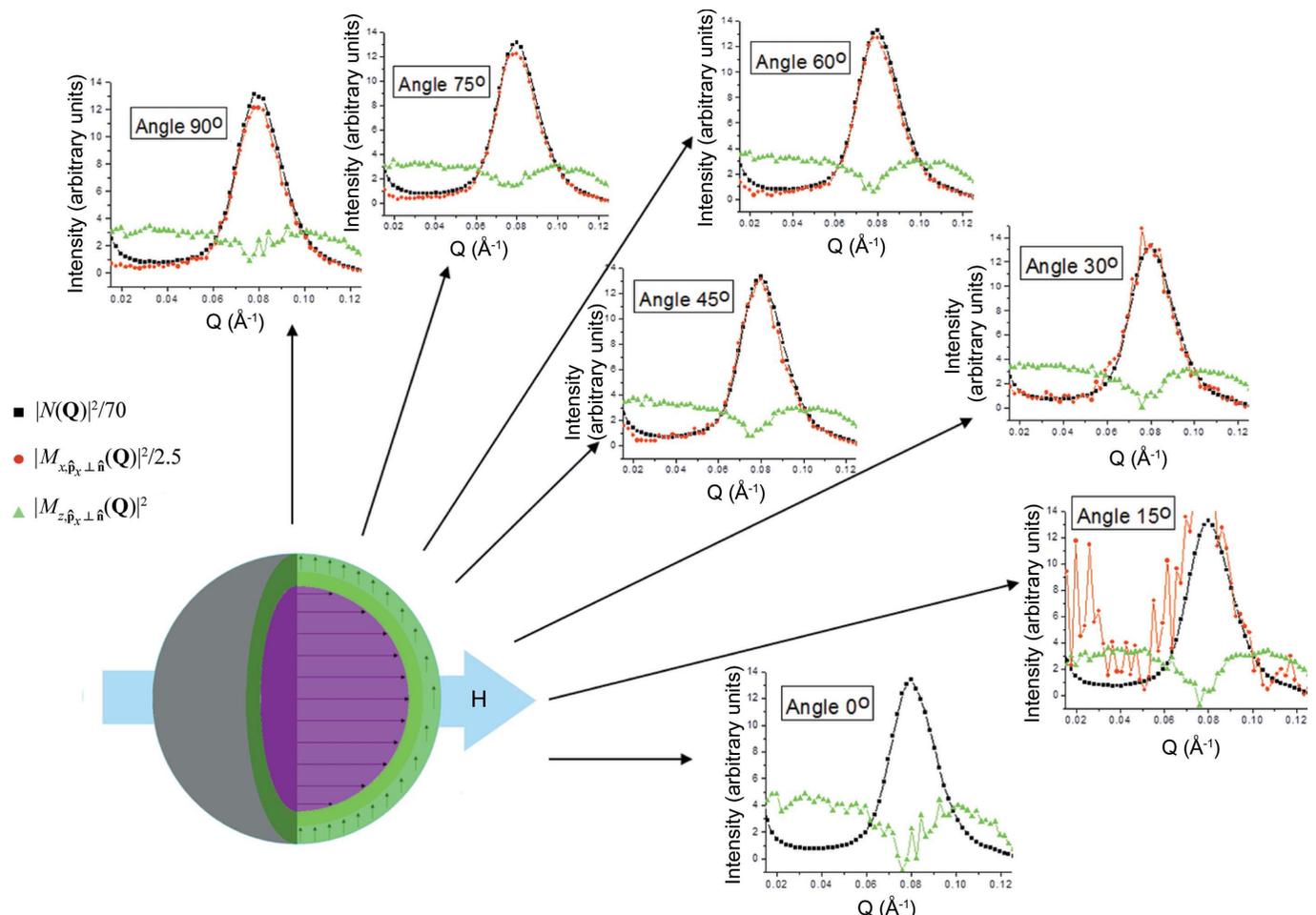- ▲ $|M_{z,\hat{\mathbf{p}}_x \perp \hat{\mathbf{n}}}(\mathbf{Q})|^2$

Figure 4
Nuclear and magnetic separation at a series of angles, using Case 8. Notice that the sample of close-packed 9 nm Fe_3O_4 nanospheres is structurally isotropic ($|N(\mathbf{Q})|^2$) and almost magnetically isotropic in both $|M_{x,\hat{\mathbf{p}}_x \perp \hat{\mathbf{n}}}(\mathbf{Q})|^2$ and $|M_{z,\hat{\mathbf{p}}_x \perp \hat{\mathbf{n}}}(\mathbf{Q})|^2$. [$|M_{x,\hat{\mathbf{p}}_x \perp \hat{\mathbf{n}}}(\mathbf{Q})|^2$ cannot be measured at $\theta = 0°$ because of the Halpern–Johnson spin selection rules.] The degree of uncertainty may be inferred from the smoothness of the curves.

$$|N(\mathbf{Q})|^2 = \tfrac{1}{2}\left\{\mathbb{A}(\mathbf{Q}) \pm \left[\mathbb{A}^2(\mathbf{Q}) - \mathbb{B}^2(\mathbf{Q})\right]^{1/2}\right\},$$
$$|M_{x,\hat{\mathbf{p}}_x\perp\hat{\mathbf{n}}}(\mathbf{Q})|^2 = \mathbb{B}^2(\mathbf{Q})/4\sin^4(\theta)\,|N(\mathbf{Q})|^2. \tag{23}$$

The requirement that $|N(\mathbf{Q})|\,|M_{y,\hat{\mathbf{p}}_x\perp\hat{\mathbf{n}}}(\mathbf{Q})|\,\overline{\cos}(\varphi_N - \varphi_{M_y,\hat{\mathbf{p}}_x\perp\hat{\mathbf{n}}}) \Rightarrow 0$ may be verified if $\mathbb{B}''(\mathbf{Q}) \Rightarrow 0$ (Table 3) and $M_{y,\hat{\mathbf{p}}_x\perp\hat{\mathbf{n}}}(\mathbf{Q})$ is known to have a net (or zero) moment. Alternatively, if the phase between $M_{y,\hat{\mathbf{p}}_x\perp\hat{\mathbf{n}}}(\mathbf{Q})$ and $N(\mathbf{Q})$ is uncertain, but it is known that $M_{y,\hat{\mathbf{p}}_x\perp\hat{\mathbf{n}}}(\mathbf{Q})$ has a net (or zero) moment, then $\mathbb{B}'$ (Table 3) may be used in place of $\mathbb{B}$ (Table 1) using (Case 8B)

$$|M_{x,\hat{\mathbf{p}}_x\perp\hat{\mathbf{n}}}(\mathbf{Q})|^2 = \mathbb{B}'^2(\mathbf{Q})/4\sin^4(\theta)\,|N(\mathbf{Q})|^2. \tag{24}$$

9.4. Cases 9A–9B: N and M_Y in phase for $\hat{\mathbf{p}} \perp \hat{\mathbf{n}}$

If $M_{y,\hat{\mathbf{p}}_x\perp\hat{\mathbf{n}}}(\mathbf{Q})$ is sufficiently long ranged so as to be in phase with $N(\mathbf{Q})$ (as could be expected if the sample were first saturated along $\mathbf{Y}$ with the magnetic spins frozen in place before the applied field along $\mathbf{Y}$ was removed and a small guide field was instead applied along $\mathbf{X}$), but $M_{x,\hat{\mathbf{p}}_x\perp\hat{\mathbf{n}}}(\mathbf{Q}) \Rightarrow 0$ or it is out of phase with $N(\mathbf{Q})$, then $M_{y,\hat{\mathbf{p}}_x\perp\hat{\mathbf{n}}}(\mathbf{Q})$ and $N(\mathbf{Q})$ may be solved from quadratic equations of $\mathbb{A}$ and $\mathbb{B}$ (Table 1) using (Case 9A)

$$|N(\mathbf{Q})|^2 = \tfrac{1}{2}\left\{\mathbb{A}(\mathbf{Q}) \pm \left[\mathbb{A}^2(\mathbf{Q}) - \mathbb{B}^2(\mathbf{Q})\right]^{1/2}\right\},$$
$$|M_{y,\hat{\mathbf{p}}_x\perp\hat{\mathbf{n}}}(\mathbf{Q})|^2 = \mathbb{B}^2(\mathbf{Q})/4\sin^2(\theta)\cos^2(\theta)\,|N(\mathbf{Q})|^2. \tag{25}$$

The requirement that $|N(\mathbf{Q})|\,|M_{x,\hat{\mathbf{p}}_x\perp\hat{\mathbf{n}}}(\mathbf{Q})|\,\overline{\cos}(\varphi_N - \varphi_{M_y,\hat{\mathbf{p}}_x\perp\hat{\mathbf{n}}}) \Rightarrow 0$ may be verified if $\mathbb{B}'(\mathbf{Q}) \Rightarrow 0$ (Table 3) and $M_{x,\hat{\mathbf{p}}_x\perp\hat{\mathbf{n}}}(\mathbf{Q})$ is known to have a net (or zero) moment. Alternatively, if the phase between $M_{x,\hat{\mathbf{p}}_x\perp\hat{\mathbf{n}}}(\mathbf{Q})$ and $N(\mathbf{Q})$ is uncertain, but it is known that $M_{x,\hat{\mathbf{p}}_x\perp\hat{\mathbf{n}}}(\mathbf{Q})$ has a net (or zero) moment, then $\mathbb{B}''$ (Table 3) may be used in place of $\mathbb{B}$ (Table 1) using (Case 9B)

$$|M_{y,\hat{\mathbf{p}}_x\perp\hat{\mathbf{n}}}(\mathbf{Q})|^2 = \mathbb{B}''^2(\mathbf{Q})/4\sin^2(\theta)\cos^2(\theta)\,|N(\mathbf{Q})|^2. \tag{26}$$

9.5. Cases 10A–10B: N in phase with both M_X and M_Y for $\hat{\mathbf{p}} \perp \hat{\mathbf{n}}$

If both $M_{x,\hat{\mathbf{p}}_x\hat{\mathbf{n}}}$ and $M_{y,\hat{\mathbf{p}}_x\hat{\mathbf{n}}}$ share coherence with $N(\mathbf{Q})$ and both contain uncompensated moments [i.e. $\overline{\cos}(\varphi_N - \varphi_{M_x,\hat{\mathbf{p}}_x\perp\hat{\mathbf{n}}}) \Rightarrow 1$ and $\overline{\cos}(\varphi_N - \varphi_{M_y,\hat{\mathbf{p}}_x\perp\hat{\mathbf{n}}}) \Rightarrow 1$, such as a sample whose form factors are magnetically equivalent from particle to particle or domain to domain], then (Case 10A)

$$N(\mathbf{Q})|^2, \beta(\mathbf{Q}) = \tfrac{1}{2}\left\{\mathbb{A}(\mathbf{Q}) \pm \left[\mathbb{A}^2(\mathbf{Q}) - \mathbb{B}^2(\mathbf{Q})\right]^{1/2}\right\},$$
$$|M_{z,\hat{\mathbf{p}}_x\perp\hat{\mathbf{n}}}(\mathbf{Q})|^2 = \mathbb{C}(\mathbf{Q}) - \beta(\mathbf{Q})/\tan^2(\theta), \tag{27}$$

where $\beta(\mathbf{Q}) \equiv |M_{x,\hat{\mathbf{p}}_x\perp\hat{\mathbf{n}}}(\mathbf{Q})|^2 \sin^4(\theta) + |M_{y,\hat{\mathbf{p}}_x\perp\hat{\mathbf{n}}}(\mathbf{Q})|^2 \cos^2(\theta) \times \sin^2(\theta) - 2|M_{x,\hat{\mathbf{p}}_x\perp\hat{\mathbf{n}}}(\mathbf{Q})|\,|M_{y,\hat{\mathbf{p}}_x\perp\hat{\mathbf{n}}}(\mathbf{Q})|\,\overline{\cos}(\varphi_{M_x,\hat{\mathbf{p}}_x\perp\hat{\mathbf{n}}} - \varphi_{M_y,\hat{\mathbf{p}}_x\perp\hat{\mathbf{n}}}) \times \sin^3(\theta)\cos(\theta) = \mathbb{B}^2(\mathbf{Q})/4|N(\mathbf{Q})|^2$. In addition, if it is known that $|M_{x,\hat{\mathbf{p}}_x\hat{\mathbf{n}}}(\mathbf{Q})|$ and $|M_{y,\hat{\mathbf{p}}_x\hat{\mathbf{n}}}(\mathbf{Q})|$ each contain net (or zero) moments, then further magnetic separation may be performed using (Case 10B)

$$|M_{z,\hat{\mathbf{p}}_x\perp\hat{\mathbf{n}}}(\mathbf{Q})|^2 = \mathbb{C}'(\mathbf{Q}) - \beta(\mathbf{Q})/\tan^2(\theta),$$
$$|M_{x,\hat{\mathbf{p}}_x\perp\hat{\mathbf{n}}}(\mathbf{Q})|^2 = \mathbb{B}'^2(\mathbf{Q})/4\sin^4(\theta)\,|N(\mathbf{Q})|^2,$$
$$|M_{y,\hat{\mathbf{p}}_x\perp\hat{\mathbf{n}}}(\mathbf{Q})|^2 = \mathbb{B}''^2(\mathbf{Q})/4\sin^2(\theta)\cos^2(\theta)\,|N(\mathbf{Q})|^2. \tag{28}$$

This simplification, and the many others that may be constructed using $\mathbb{B}'$ and $\mathbb{B}''$ or $\mathbb{C}'$ and $\mathbb{C}''$ (Table 3) in place of $\mathbb{B}$ or $\mathbb{C}$ (Table 1), should only be applied to samples that are known to be symmetric with respect to $\hat{\mathbf{p}}$.

10. Experimental angular resolution demonstration

To illustrate an experimental application of the equations in Table 4 for performing angular analysis, let us return once again to the scattering patterns from randomly oriented, close-packed crystallites composed of 9 nm Fe_3O_4 nanospheres in an applied saturating field of 1.25 T. $|N(|\mathbf{Q}|, 0°)|^2$, obtained using the most general case (Case 3, Table 4), and $|M_{x,\hat{\mathbf{p}}_x\perp\hat{\mathbf{n}}}(|\mathbf{Q}|, 90°)|^2$, obtained using Case 4 (Table 4) with the assumption that the sample was structurally isotropic, were each dominated by Bragg peaks as shown in Fig. 4. Combined with $|M_{z,\hat{\mathbf{p}}_x\perp\hat{\mathbf{n}}}(|\mathbf{Q}|, 90°)|^2$, obtained using Case 3 (Table 4), this separation revealed a canted magnetic shell structure (Krycka et al., 2010). One may well ask whether this shell is truly isotropic in nature, as postulated. To answer this question, we apply Case 8A of Table 4 to solve for $|N(\mathbf{Q})|^2$ and $|M_{x,\hat{\mathbf{p}}_x\perp\hat{\mathbf{n}}}(\mathbf{Q})|^2$ at arbitrary θ. With $|N(\mathbf{Q})|^2$ solved at all θ, $|M_{z,\hat{\mathbf{p}}_x\perp\hat{\mathbf{n}}}(\mathbf{Q})|^2$ is extracted using $\mathbb{A}$ and $\mathbb{C}$ (Table 1) in conjunction with Case 3 (Table 4). It should be noted that an infinitely small slice of experimental data cannot be taken about a specific angle as the data set soon becomes statistically noise limited. Thus, for practical purposes we have taken $\pm 10°$ sector slices about an angle θ of interest. To compensate for the angular dependence inherent in the $\hat{\mathbf{p}}_x \perp \hat{\mathbf{n}}$ geometry, we utilize the following integrations (where α and β correspond to the $\pm$ angular limits):

$$\int_\alpha^\beta \tan^2(\theta)\,d\theta = [\tan(\beta) - \tan(\alpha) - \beta + \alpha]\frac{1}{\beta - \alpha},$$

$$\int_\alpha^\beta \sin^2(\theta)\cos^2(\theta)\,d\theta = \left[\frac{\beta - \alpha}{8} - \frac{\sin(4\beta) - \sin(4\alpha)}{32}\right]\frac{1}{\beta - \alpha},$$

$$\int_\alpha^\beta \sin^4(\theta)\,d\theta = \left[\frac{3(\beta - \alpha)}{8} + \frac{\sin(4\beta) - \sin(4\alpha)}{32}\right.$$
$$\left. - \frac{\sin(2\beta) - \sin(2\alpha)}{4}\right]\frac{1}{\beta - \alpha},$$

$$\int_\alpha^\beta \cos^4(\theta)\,d\theta = \left[\frac{3(\beta - \alpha)}{8} + \frac{\sin(4\beta) - \sin(4\alpha)}{32}\right.$$
$$\left. + \frac{\sin(2\beta) - \sin(2\alpha)}{4}\right]\frac{1}{\beta - \alpha}. \tag{29}$$

The results are presented in Fig. 4.

It is immediately obvious that $|N(\mathbf{Q})|^2$ remains nearly constant with angle, thus confirming the structurally isotropic nature of this sample. $|M_{x,\hat{\mathbf{p}}_x \perp \hat{\mathbf{n}}}(\mathbf{Q})|^2$, though fairly uniform as a function of angle, does increase slightly in going from $\theta = 90°$ to $\theta = 0°$. The interference between $N(\mathbf{Q})$ and $M_{x,\hat{\mathbf{p}}_x \perp \hat{\mathbf{n}}}(\mathbf{Q})$ is likely to be more strongly correlated along the applied field direction than perpendicular to it, and could explain the variation of $|M_{x,\hat{\mathbf{p}}_x \perp \hat{\mathbf{n}}}(\mathbf{Q})|^2$. Extraction of $|M_{z,\hat{\mathbf{p}}_x \perp \hat{\mathbf{n}}}(\mathbf{Q})|^2$ appears to flatten slightly for θ approaching $90°$. This may mean that the $|M_{z,\hat{\mathbf{p}}_x \perp \hat{\mathbf{n}}}(\mathbf{Q})|^2$ morphology (form factor) is slightly less uniform in the $\mathbf{Y}$ direction than the $\mathbf{X}$ direction, or that the short-range structure factor differs slightly along $\mathbf{Y}$ *versus* $\mathbf{X}$. However, since the same general shape and scattering magnitude are maintained, this suggests that the basic morphology remains nearly isotropic. The main point, however, is that a full angular analysis can be obtained in accordance with Table 4.

11. Conclusions

Polarization-analyzed SANS is a powerful tool that can be employed in the study of magnetic interactions with the ability to resolve three-dimensional magnetism. However, such experiments often produce a wealth of structural and magnetic information that can be challenging to disentangle in the realm of anisotropic materials, such as biologically relevant magnetic systems in solution, magnetostrictive materials, and patterned or crystalline samples with intrinsic structural anisotropy. Building upon previous work (Moon *et al.* 1969; Schärpf & Capellmann, 1993; Wiedenmann, 2005; Michels & Weissmüller, 2008) and applying basic symmetry arguments, we discuss how various phase relationships between structural and magnetic interference terms influence the symmetry patterns observed (Table 3). We also outline straightforward analytic procedures (Table 4) for separating the structural and magnetic components in the most common experimental conditions. This contribution should thus serve as a handy reference for experimentalists trying to determine how to best reduce their polarization-analyzed SANS (PASANS) results. It is clear that PASANS has entered an exciting growth phase, owing largely to advances in polarized ^{3}He spin filters capable of analyzing divergently scattered beams (Petoukhov *et al.*, 2006; Babcock *et al.*, 2007; Keiderling *et al.*, 2008; Chen *et al.*, 2009), and this technique may well prove vital in understanding the collective behavior of many magnetic systems on the nanoscale.

References

Babcock, E., Petoukhov, A., Chastagnier, J., Jullien, D., Lelièvre-Berna, E., Andersen, K. H., Georgii, R., Masalovich, S., Boag, S., Frost, C. D. & Parnell, S. R. (2007). *Physica B*, **397**, 172–175.

Blume, M. (1963). *Phys. Rev.* **130**, 1670–1676.

Brown, P. J. (2001). *Physica B*, **297**, 198–203.

Chang, L. J., Su, Y., Kao, Y.-J., Chou, Y. Z., Mittal, R., Schneider, H., Brückel, Th., Balakrishnan, G. & Lees, M. R. (2010). *Phys. Rev. B*, **82**, 172403.

Chatterji, T. (2006). *Neutron Scattering from Magnetic Materials*. Amsterdam: Elsevier.

Chen, W. C., Erwin, R., McIver, J. W. III,, Watson, S., Fu, C. B., Gentile, T. R., Borchers, J. A., Lynn, J. W. & Jones, G. L. (2009). *Physica B*, **404**, 2663–2666.

Cywinski, R., Kilcoyne, S. & Stewart, J. (1999). *Physica B*, **267–268**, 106–114.

Dufour, C., Fitzsimmons, M. R., Borchers, J. A., Laver, M., Krycka, K. L., Dumesnil, K., Watson, S. M., Chen, W. C., Won, J. & Singh, S. (2011). *Phys. Rev. B*, **84**, 064420.

Feygenson, M., Schweika, W., Ioffe, A., Vakhrushev, S. B. & Brückel, T. (2010). *Phys. Rev. B*, **81**, 064423.

Gaspar, A. M., Busch, S., Appavou, M.-S., Haeussler, W., Georgii, R., Su, Y. & Doster, W. (2010). *Biochim. Biophys. Acta*, **1804**, 76–82.

Gentile, T. R., Jones, G. L., Thompson, A. K., Barker, J., Glinka, C. J., Hammouda, B. & Lynn, J. W. (2000). *J. Appl. Cryst.* **33**, 771–774.

Halpern, O. & Johnson, M. H. (1939). *Phys. Rev.* **55**, 898–923.

Honecker, D., Döbrich, F., Dewhurst, C. D., Wiedenmann, A. & Michels, A. (2011). *J. Phys. Condens. Matter*, **23**, 016003.

Jones, G. L., Dias, F., Collett, B., Chen, W. C., Gentile, T. R., Piccoli, P. M. B., Miller, M. E., Schultz, A. J., Yan, H., Tong, X., Snow, W. M., Lee, W. T., Hoffmann, C. & Thomison, J. (2006). *Physica B*, **385**, 1131–1133.

Keiderling, U. (2002). *Appl. Phys. A*, **74**, S1455–S1457.

Keiderling, U., Wiedenmann, A., Rupp, A., Klenke, J. & Heil, W. (2008). *Meas. Sci. Technol.* **19**, 034009.

Krycka, K. L., Booth, R. A., Hogg, C. R., Ijiri, Y., Borchers, J. A., Chen, W. C., Watson, S. M., Laver, M., Gentile, T. R., Dedon, L. R., Harris, S., Rhyne, J. J. & Majetich, S. A. (2010). *Phys. Rev. Lett.* **104**, 207203.

Krycka, K., Chen, W., Borchers, J., Maranville, B. & Watson, S. (2012). *J. Appl. Cryst.* **45**, 546–553.

Laver, M., Mudivarthi, C., Cullen, J. R., Flatau, A. B., Chen, W.-C., Watson, S. M. & Wuttig, M. (2010). *Phys. Rev. Lett.* **105**, 027202.

Löffler, J. F., Braun, H. B., Wagner, W., Kostorz, G. & Wiedenmann, A. (2005). *Phys. Rev. B*, **71**, 134410.

Majkrzak, C. (1991). *Handbook of Neutron Scattering*. Berlin: Springer-Verlag.

Maleyev, S. V. (2004). *J. Phys. Condens. Matter*, **16**, S899.

Maleyev, S. V., Baryakhtar, V. G. & Suris, R. A. (1963). *Sov. Phys. Solid State*, **4**, 2533–2540.

Michels, A. & Weissmüller, J. (2008). *Rep. Prog. Phys.* **71**, 066501.

Moon, R. M., Riste, T. & Koehler, W. C. (1969). *Phys. Rev.* **181**, 920–931.

Ogrin, F. Y., Lee, S. L., Wismayer, M., Thomson, T., Dewhurst, C. D., Cubitt, R. & Weekes, S. M. (2006). *J. Appl. Phys.* **99**, 08G912.

Petoukhov, A. K., Andersen, K. H., Jullien, D., Babcock, E., Chastagnier, J., Chung, R., Humblot, H., Lelièvre-Berna, E., Tasset, F., Radu, F., Wolff, M. & Zabel, H. (2006). *Physica B*, **385–386**, 1146–1148.

Saranu, S., Grob, A., Weissmüller, J. & Herr, U. (2008). *Phys. Status Solidi A*, **205**, 1774–1778.

Schärpf, O. & Capellmann, H. (1993). *Phys. Status Solidi A*, **135**, 359–379.

Schweika, W. (2010). *J. Phys. Conf. Ser.* **211**, 012026.

Tasset, F. (1989). *Physica B*, **156–157**, 627–630.

Wiedenmann, A. (2005). *Physica B*, **356**, 246–253.

Wildes, A. R. (2006). *Neutron News*, **17**(2), 17–25.